A domain decomposition approach to finite-epsilon homogenization of scalar transport in porous media

Yohan Davit, Fabrice Golfier, Jean-Claude Latché, Michel Quintard

SIAM J. APPL. MATH.
Vol. 79, No. 5, pp. 1797–1822

A DOMAIN DECOMPOSITION APPROACH TO FINITE-EPSILON HOMOGENIZATION OF SCALAR TRANSPORT IN POROUS MEDIA*

YOHAN DAVIT†, FABRICE GOLFIER‡, JEAN-CLAUDE LATCHÉ§, AND MICHEL QUINTARD†

Abstract. Modeling scalar transport by advection and diffusion in multiscale porous structures is a challenging problem, particularly in the preasymptotic regimes when non-Fickian effects are prominent. Mathematically, one of the main difficulties is to obtain macroscale models from the homogenization of conservation equations at microscale when epsilon, the ratio of characteristic lengthscales between the micro- and macroscale, is not extremely small compared to unity. Here, we propose the basis of a mathematical framework to do so. The focal idea is to decompose the spatial domain at pore-scale into a set of N subdomains to capture characteristic times associated with exchanges between these subdomains. At macroscale, the corresponding representation consists of a system of N coupled partial differential equations describing the transport of the spatially averaged scalar variable within each subdomain. Besides constructing the framework, we also compare numerically the results of our models to a complete resolution of the problem at the pore-scale, which shows great promises for capturing preasymptotic regimes, non-Fickian transport, and going toward finite-epsilon homogenization.

Key words. non-Fickian, scalar transport, advection and diffusion, porous media, domain decomposition, spatial averaging

AMS subject classifications. 76S99, 76R99

DOI. 10.1137/17M1157775

1. Introduction.

In most structures displaying multiscale heterogeneities, such as porous media, the complexity of the geometry often prevents the computation of conservation laws at the smallest scales. A standard solution to this consists in filtering out the high-frequency fluctuations contained in the microscale details and adopting a homogenized point of view. In porous media, a famous example of one such model is Darcy's law describing momentum transport using the gradient of the spatially averaged pressure, a filtration velocity, and a permeability. Obtaining the average equations directly from fundamental principles at the microscale can be performed using a number of mathematical approaches, including homogenization theories (HTs [30, 46, 5, 48]) often based on multiscale asymptotics (MA) and the volume averaging theory (VAT [52, 26]). For linear problems and locally periodic structures, VAT and HT often yield very similar macroscale equations in which effective parameters, such as the permeability, can be calculated by solving closure problems in a unit-cell.

With these two techniques, the macroscale model represents an asymptotic limit of the partial differential equations describing conservation laws at the microscale. For MA, this is formalized by studying a sequence of problems in the limit where the ratio between the microscopic and macroscopic lengthscales, ε, goes to zero.

*Received by the editors November 20, 2017; accepted for publication (in revised form) July 2, 2019; published electronically September 17, 2019.
https://doi.org/10.1137/17M1157775

†Institut de Mécanique des Fluides de Toulouse (IMFT), Université de Toulouse, CNRS, INPT, UPS, Toulouse, France (yohan.davit@imft.fr, michel.quintard@imft.fr).

‡University of Lorraine/CNRS/CREGU, GeoRessources Laboratory, Vandoeuvre-les-Nancy, France (fabrice.golfier@ensg.univ-lorraine.fr).

§Institut de Radioprotection et de Sûreté Nucléaire (IRSN), Saint-Paul-Lez-Durance, France (jean-claude.latche@irsn.fr).

Constraints regarding the scaling of dimensionless numbers are also necessary in order to further account for the fact that a real physical system is associated with only one finite value of ε. To illustrate this point, consider Taylor's dispersion of a solute in a fluid flowing through a tube (Poiseuille velocity profile) of radius R and length L, with a cross-section average velocity $\langle v \rangle$ and a molecular diffusion coefficient D. In this configuration, the standard homogenized description is an advection-dispersion equation with a dispersion coefficient that depends on the square of the Péclet number (dimensionless time $t' = {}^{tR^2}/_{D}$ and space $x' = {}^{x}/_{R}$). This result, however, is only valid asymptotically when each solute molecule has had time to visit the whole section of the tube before reaching its end (more details about Taylor's dispersion in [50, 2, 3] and about the convergence in [12, 55, 54]). This constraint can be expressed in terms of the characteristic time for radial diffusion, ${}^{R^2}/_{D}$, which must be much smaller than the time for longitudinal advection, ${}^{L}/_{\langle v \rangle}$. In dimensionless form, we can write this constraint as $\varepsilon \mathrm{Pe} \ll 1$ where $\varepsilon = {}^{R}/_{L}$ and the Péclet number is defined as $\mathrm{Pe} = {}^{\langle v \rangle R}/_{D}$. For a finite value of ε, this means that we must have $\mathrm{Pe} \ll \varepsilon^{-1}$ and that the homogenized model will not describe accurately transport when the Péclet number is too large, i.e., when $\mathrm{Pe} = \mathcal{O}\left(\varepsilon^{-n}\right)$ with $n > 1$. Overcoming this limitation and deriving homogenized models that hold for large Péclet numbers and any finite value of ε is an important challenge in applied mathematics, one that remains unsolved.

In this paper, we propose an idea to do so and develop the corresponding mathematical framework using the VAT, which is based on a domain decomposition of the microscale domain. The focal concept is that the domain of interest can be decomposed into a finite set of subdomains spanning the whole domain and that the number of subdomains, N, can be used to control the small parameter, therefore relaxing constraints in the standard HT or VAT. For example, for the case of Taylor's dispersion, we could decompose the fluid in the tube into a nested set of coaxial tubes. Our method would lead to a macroscale representation with a system of N coupled equations, each equation describing the average concentration within each portion of the tube. The idea underlying this decomposition is that the homogenized model may now hold when each molecule of solute has had time to visit each subdomain independently, not the whole fluid phase. For a given value of the diffusion coefficient, this time depends directly on the size of these subdomains, which is controlled by N. The constraint would now be that the time for radial diffusion within each subdomain, $\frac{R^2}{N^2 D}$, must be much smaller than the longitudinal time for advection within each subdomain. For each subdomain α, this yields the inequality $\frac{\varepsilon}{N}\mathrm{Pe}^{(\alpha)} \ll 1$, with the $\mathrm{Pe}^{(\alpha)}$ the Péclet number associated with the subdomain α, so that we need $\max_{\alpha}(\frac{\varepsilon}{N}\mathrm{Pe}^{(\alpha)}) \ll 1$ instead of $\varepsilon \mathrm{Pe} \ll 1$. The difference between these two expressions is that, for a finite value of ε, we can define the small parameter as $\delta = \frac{\varepsilon}{N}$, which in theory can be made as small as needed by increasing the number of subdomains, N. This can be extended to any locally periodic heterogeneous material where the unit-cell is decomposed into a set of N subdomains. Of course, this is just the intuitive idea of our developments and we will study the effect of N in more detail numerically in model cases.

Another angle on this problem emerges from the consideration of real systems, which we know often display non-Fickian effects at the macroscale. For example, breakthrough curves describing the response of a geological formation to an impulse concentration often feature tailing effects that cannot be captured by an advection-dispersion equation [33, 7, 6, 8, 25, 17, 15]. This type of behavior is often attributed to heterogeneities at various scales, for instance, it will occur when the properties of the medium, for instance, the diffusion or permeability coefficients, display

distributions with large variances. Further, boundary conditions, nonlinearities, source terms, topological effects, or transient phenomena can generate or amplify nonequilibrium effects—large gradients at the microscale—leading to non-Fickian transport. Several approaches [16, 36] are used to describe these phenomena, including stochastic [23], nonlocal [31], higher-order, multirate mass transfer (MRMT) [27, 4, 53] and multicontinua models (e.g., mobile-mobile, mobile-immobile, dual-porosity, or dual-permeability). For MRMT and multicontinua models, the central point is the introduction of characteristic times that describe exchanges between different subdomains at the microscale by coupling equations representing each phase separately, as is the case of our approach. However, a mathematical basis, as the one associated with HTs and upscaling, defining clearly the contours of such models is still lacking.

Several non-Fickian transport models have been obtained using both the MA and VATs, but these only apply to specific cases and lack generality. For instance, mobile-immobile models have been developed using HT in the case where the unit-cell contains two different domains that differ by the value of the diffusion coefficients [30, 29]. The approach relies on the constraint that these diffusion coefficients are several orders of magnitude different, which is formalized using a scaling of the ratio between both diffusion coefficients in ε. With the VAT, formulations with two equations (one for each domain, and exchange terms between the two) have been obtained by treating the case of two phases connected via transmission (boundary) conditions [1, 32, 14, 13, 35, 38, 44, 20]. Such models seem to be more general as nonequilibrium effects can be postulated as a working hypothesis without the need to identify a priori the origin of the gradients. These could originate from a particular scaling of dimensionless numbers, but also from non-linearities, boundary, initial, or reactive conditions. Another important aspect of these two-equation models obtained using VAT is that they (1) feature counterintuitive (nondiagonal) coupling terms for the advective and diffusive operators, which are not present in heuristic MRMT models, and (2) they can be easily extended to many situations such as mobile-mobile or reactive conditions, which is not necessarily the case of MRMT because of the lack of link with the microscale physics.

One of the limitations of the VAT approach, which we overcome in this paper, is that there exists no general theory that deals with any number of subdomains, as is the case for empirical MRMT models [4]. Further, the nonequilibrium approach with the two-equation model is mostly used when two distinct physical phases (when the microscale is the pore-scale) or regions (when the microscale is the Darcy-scale in heterogeneous systems) can be identified [44], which is limiting. An important question is therefore: Can we still apply the same idea and perform the domain decomposition independently of the number of physical phase or region in order to derive a theory that overcomes the limitations associated with finite-ε problems and scalings of dimensionless numbers? For instance, it was shown for momentum transport that even one physical phase can be decomposed into two fluids [47]. Of course, the problem for momentum transport is not the same as the one for scalar transport that we study here; however, this is a clue suggesting that there is not necessarily a link between the number of physical phases and the number of subdomains that is relevant for upscaling.

Here, our goal is to develop a sound physical and mathematical background for models containing any number N of subdomains. We will also look at toy problems to figure out if there is hope that this may be used to overcome limitations of standard homogenized representations. For simplicity, we focus on a generic linear advection-diffusion problem of a scalar quantity in a locally periodic medium, this problem

having direct applications in a number of important problems such as solute transport in heterogeneous multiscale materials (e.g., porous or biological media), heat transfer in composites, or flow in large-scale geological formations. We first define (section 2) the microscale problem and corresponding operator notation. We then use a modified form of the VAT in section 3 to derive a macroscale model for any number N of subdomains. Finally, we go on to test our approach for model dispersion problems (section 4) and compare our results for two- and three-equation models with direct numerical simulation at the microscale.

2. Definitions and microscale problem.

2.1. Problem definition and notation. The spatial domain of interest (see Figure 2.1) is a set $\Omega \subset \mathbb{R}^n$ that is characterized by a lengthscale L and boundary $\partial\Omega$. This domain is locally periodic with unit-cell Y, which has dimensions $\ell_1 \times \cdots \times \ell_n$ and is characterized by a lengthscale ℓ (a mean value of $\ell_{i\in[1,n]}$, for instance). We further decompose Y into N subdomains $Y^{(\alpha)}$ with $\alpha \in [1, N]$. The interior boundary of each subdomain $Y^{(\alpha)}$ is noted $\partial Y^{(\alpha)}$ and boundaries between subdomains $Y^{(\alpha)}$ and $Y^{(\beta)}$ are noted $\partial Y^{(\alpha\beta)} = \partial Y^{(\alpha)} \cap \partial Y^{(\beta)}$. The domain decomposition extends to the entire domain Ω by periodicity and we write $\Omega^{(\alpha)} = \bigcup Y^{(\alpha)}$. Similarly, we also define $\partial\Omega^{(\alpha)} = \bigcup \partial Y^{(\alpha)}$ and $\partial\Omega^{(\alpha\beta)} = \bigcup \partial Y^{(\alpha\beta)}$.

We consider the following linear partial differential equation:

$$\partial_t u + \mathcal{L}u = 0 \text{ in } \Omega \times \mathbb{R}, \tag{2.1}$$

where $\mathcal{L}$ is an advection-diffusion operator such that

$$\mathcal{L}u \equiv \mathbf{v}(\mathbf{x}) \cdot \boldsymbol{\nabla} u - \boldsymbol{\nabla} \cdot (\mathbf{A}(\mathbf{x}) \cdot \boldsymbol{\nabla} u). \tag{2.2}$$

We do not detail the boundary conditions on $\partial\Omega$ here as they are not needed for the formal upscaling developments. Alternatively, this can be written in indicial form as

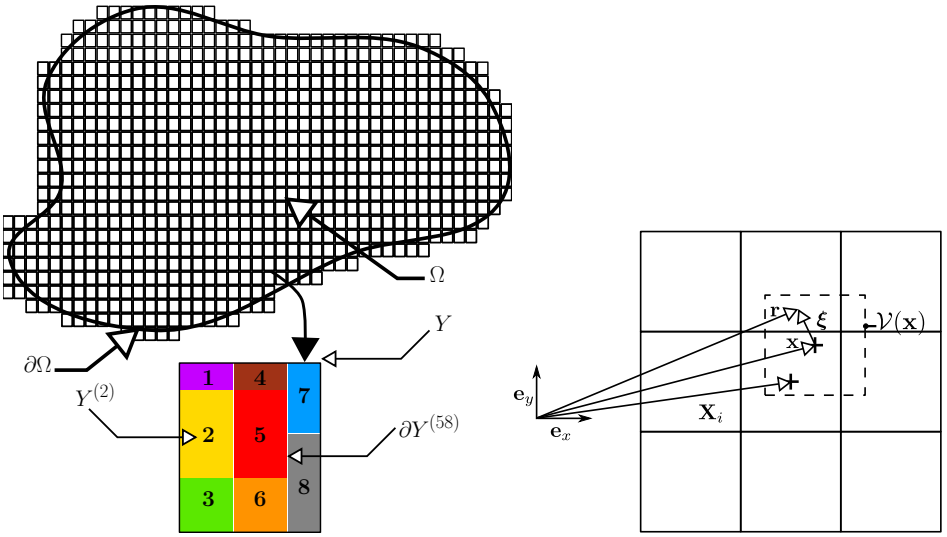

FIG. 2.1. *The picture on the left-hand side shows schematics of a domain, $\Omega \subset \mathbb{R}^2$, the unit-cell, Y, decomposed into $N = 8$ subdomains, $Y^{(\alpha)}$. The picture on the right-hand side represents an example averaging volume $\mathcal{V}(\mathbf{x})$ centered at point $\mathbf{x}$, the vector pointing within the averaging volume, $\boldsymbol{\xi} = \mathbf{r} - \mathbf{x}$, and the center of unit-cell i, $\mathbf{X}_i$.*

$$\mathcal{L}u = v_i(\mathbf{x})\,\partial_i u - \partial_i\left(\mathsf{A}_{ij}(\mathbf{x})\,\partial_j u\right), \tag{2.3}$$

with the summation convention over repeated indices. The velocity field $\mathbf{v}(\mathbf{x})$ satisfies the incompressibility condition, $\boldsymbol{\nabla}\cdot\mathbf{v}=0$. $\mathbf{A}(\mathbf{x})$ is a periodic symmetric coercive dyadic field. For simplicity, we treat the variability in space implicitly in the remainder of this paper and simply write $\mathbf{v}$ and $\mathbf{A}$ instead of $\mathbf{v}(\mathbf{x})$ and $\mathbf{A}(\mathbf{x})$. We also define a flux operator $\boldsymbol{\mathcal{J}}$ such that

$$\boldsymbol{\mathcal{J}}u \equiv \mathbf{v}u - \mathbf{A}\cdot\boldsymbol{\nabla}u, \tag{2.4}$$

and $\mathcal{L}u = \boldsymbol{\nabla}\cdot\boldsymbol{\mathcal{J}}u$.

Finally, we consider the equivalent domain decomposition problem with transmission boundary conditions,

$$\partial_t u^{(\alpha)} + \mathcal{L}^{(\alpha)}u^{(\alpha)} = 0 \text{ in } \Omega^{(\alpha)}\times\mathbb{R}, \tag{2.5}$$

$$[\![u]\!]^{(\alpha\beta)} = 0 \text{ on } \partial\Omega^{(\alpha\beta)}\times\mathbb{R}, \tag{2.6}$$

$$\mathbf{n}^{(\alpha\beta)}\cdot[\![\boldsymbol{\mathcal{J}}u]\!]^{(\alpha\beta)} = 0 \text{ on } \partial\Omega^{(\alpha\beta)}\times\mathbb{R}, \tag{2.7}$$

where $\alpha,\beta\in[1,N]$ with $\alpha\neq\beta$, $[\![g]\!]^{(\alpha\beta)}\equiv g^{(\alpha)}-g^{(\beta)}$ is a jump notation and

$$\mathcal{L}^{(\alpha)} \equiv \mathbf{v}^{(\alpha)}\cdot\boldsymbol{\nabla}u^{(\alpha)} - \boldsymbol{\nabla}\cdot\left(\mathbf{A}^{(\alpha)}\cdot\boldsymbol{\nabla}u^{(\alpha)}\right), \tag{2.8}$$

with $\mathbf{v}^{(\alpha)}$ and $\mathbf{A}^{(\alpha)}$ are restrictions of, respectively, $\mathbf{v}$ and $\mathbf{A}$ from Ω to $\Omega^{(\alpha)}$. This formulation is completely equivalent to (2.1) but is going to be the starting point for developing the N-equation formulation.

2.2. Averaging notation and perturbation decomposition. To homogenize the transport equations, we first need to define the spatial averaging operator. The most general formulation is a spatial convolution as discussed in [39, 40, 43, 42, 41, 21, 34]. The average of $u^{(\alpha)}$ evaluated at point $\mathbf{x}$ reads

$$\left\langle u^{(\alpha)}\right\rangle\Big|_{\mathbf{x}} \equiv \int_{\mathbb{R}^n} m(\mathbf{x}-\mathbf{r})\,\chi^{(\alpha)}(\mathbf{r})\,u(\mathbf{r})\,d\mathbf{r}, \tag{2.9}$$

which we can simply write as

$$\left\langle u^{(\alpha)}\right\rangle\Big|_{\mathbf{x}} \equiv m * \left(\chi^{(\alpha)}u\right)\Big|_{\mathbf{x}} \tag{2.10}$$

with m a kernel normalized so that $\int_{\mathbb{R}^n} m = 1$ and $\chi^{(\alpha)}$ the fluid-phase indicator function, whose value is 1 in the subdomain α and 0 otherwise. In applying the convolution, there is of course an issue in the vicinity of $\partial\Omega$. There are a number of ways this problem can be solved (see, for instance, [37]), at least formally.

The role of the convolution is to act as a low-pass filter, eliminating lengthscales that are smaller than or equal to the size of the unit-cell ℓ. The definition of the averaging operator using convolutions is fundamental to control properties of the average fields, the smoothness in particular, by adequately choosing the kernel m. For simplicity and because this is not the subject of this paper, we assume that the averaging operator is ideal with regard to the volume averaging procedure (see [21] for more details), i.e., that

1. m is symmetric regarding each spatial direction,
2. $m \in C^k(\mathbb{R}^n)$ with k the order of the closure and of the Taylor series expansions used in volume averaging,
3. the averaging operator, $\langle \bullet \rangle$, is idempotent and if g is periodic with unit-cell Y, then $\langle g \langle u^{(\alpha)} \rangle \rangle|_{\mathbf{x}} = \langle g \rangle|_{\mathbf{x}} \langle u^{(\alpha)} \rangle|_{\mathbf{x}}$,
4. if g is periodic with unit-cell Y, then $m * g(\mathbf{x}) = m_{\sqcap} * g(\mathbf{x})$ with $m_{\sqcap} = \prod_{i=1}^{n} R(x_i)$ the standard averaging kernel and R the one-dimensional rectangular function.

We now define the porosity of the domain α as $\phi_\alpha \equiv \langle 1 \rangle|_{\mathbf{x}} = m * \chi^{(\alpha)}(\mathbf{x})$. Since $\chi^{(\alpha)}$ is periodic, we also have $\phi_\alpha = m_{\sqcap} * \chi^{(\alpha)}(\mathbf{x})$ using property 4 above. The intrinsic average of $u^{(\alpha)}$ is

$$\mathcal{U}_\alpha|_{\mathbf{x}} \equiv \frac{m * \left(\chi^{(\alpha)} u\right)}{m * \chi^{(\alpha)}}(\mathbf{x}) = \frac{m * \left(\chi^{(\alpha)} u\right)}{\phi_\alpha}(\mathbf{x}) \tag{2.11}$$

so that we have the relationship

$$\mathcal{U}_\alpha = \phi_\alpha^{-1} \left\langle u^{(\alpha)} \right\rangle \tag{2.12}$$

and can define a pertubation decomposition as

$$u^{(\alpha)} \equiv \mathcal{U}_\alpha + \tilde{u}^{(\alpha)}. \tag{2.13}$$

The idea in using such a perturbation is to separate the spatial frequencies of the field, with $\mathcal{U}_\alpha$ containing only low-frequency variations.

3. Upscaling via volume averaging. The first step of the method consists in applying the averaging operator to each subdomain. Since all subdomains are immobile, this operation yields, for any point in Ω, the following average equation for each subdomain α:

$$\partial_t \mathcal{U}_\alpha + \phi_\alpha^{-1} \left\langle \mathcal{L}^{(\alpha)} u^{(\alpha)} \right\rangle = 0. \tag{3.1}$$

3.1. Perturbations. The second step is the subtraction of (3.1) from (2.5). This operation yields the following perturbation equations, for any point in $\Omega^{(\alpha)}$:

$$\partial_t \tilde{u}^{(\alpha)} + \widetilde{\mathcal{L}}^{(\alpha)} u^{(\alpha)} = 0, \tag{3.2}$$

where the notation $\widetilde{\mathcal{L}}^{(\alpha)} u^{(\alpha)} \equiv \mathcal{L}^{(\alpha)} u^{(\alpha)} - \phi_\alpha^{-1} \left\langle \mathcal{L}^{(\alpha)} u^{(\alpha)} \right\rangle$ is a generalization of the perturbation notation for u to partial differential operators. Upon assuming quasi stationarity of this problem (this issue is not discussed in detail here as it is a standard assumption used in most techniques [52, 10, 5] and can also be relaxed by introducing time convolutions [20, 18, 19]) and using the perturbation decomposition (2.13), we can simplify the problem as

$$\widetilde{\mathcal{L}}^{(\alpha)} \tilde{u}^{(\alpha)} = -\widetilde{\mathcal{L}}^{(\alpha)} \mathcal{U}_\alpha, \tag{3.3}$$

along with the boundary conditions on $\partial\Omega^{(\alpha\beta)}$,

$$[\![\tilde{u}]\!]^{(\alpha\beta)} = -\left(\mathcal{U}_\alpha - \mathcal{U}_\beta\right), \tag{3.4}$$

$$\mathbf{n}^{(\alpha\beta)} \cdot [\![\boldsymbol{\mathcal{J}} \tilde{u}]\!]^{(\alpha\beta)} = -\mathbf{n}^{(\alpha\beta)} \cdot \left(\boldsymbol{\mathcal{J}}^{(\alpha)} \mathcal{U}_\alpha - \boldsymbol{\mathcal{J}}^{(\beta)} \mathcal{U}_\beta\right). \tag{3.5}$$

3.2. Approximate form of the solution. The next step is to postulate an approximate form of the perturbation problem. Considering average terms as sources in the perturbation equations, (3.3) to (3.5), suggests an approximation in the form

$$\tilde{u}^{(\alpha)} = \left(a_j^{(\alpha)} - \delta_{\alpha j}\right)\mathcal{U}_j + \mathbf{b}_j^{(\alpha)} \cdot \boldsymbol{\nabla}\mathcal{U}_j + \text{h.o.t.}, \tag{3.6}$$

where we have used the summation convention over repeated indices j, $\delta_{\alpha j}$ is the Kronecker symbol, and h.o.t. is an abbreviation for higher-order terms. In these equations, $a_j^{(\alpha)}$ are scalars and $\mathbf{b}_j^{(\alpha)}$ are first-order tensors. We therefore construct our approximate solution for the scalar field as

$$u^{(\alpha)} = a_j^{(\alpha)}\mathcal{U}_j + \mathbf{b}_j^{(\alpha)} \cdot \boldsymbol{\nabla}\mathcal{U}_j, \tag{3.7}$$

and for the flux, we write

$$\boldsymbol{\mathcal{J}}^{(\alpha)}u^{(\alpha)} = \left(\boldsymbol{\mathcal{J}}^{(\alpha)}a_j^{(\alpha)}\right)\mathcal{U}_j + \left(\boldsymbol{\mathcal{J}}^{(\alpha)}\mathbf{b}_j^{(\alpha)} - \mathbf{A}a_j^{(\alpha)}\right) \cdot \nabla\mathcal{U}_j. \tag{3.8}$$

3.3. Closure problems. We then inject (3.7) and (3.8) into (3.3). Since, by construction, (3.7) must be correct for any value of $\mathcal{U}_j$ and $\nabla\mathcal{U}_j$, we can identify each problem associated with $\mathcal{U}_j$ and $\nabla\mathcal{U}_j$ to obtain a set of problems that are usually termed closure problems. In fact, it is exactly for this reason that we postulated this form of perturbation. For terms corresponding to $\mathcal{U}_j$, we have

$$\widetilde{\mathcal{L}}^{(\alpha)}a_j^{(\alpha)} = 0 \tag{3.9}$$

with conditions

$$[\![a_j]\!]^{(\alpha\beta)} = 0 \text{ on } \partial Y^{(\alpha\beta)}, \tag{3.10}$$

$$\mathbf{n}^{(\alpha\beta)} \cdot [\![\boldsymbol{\mathcal{J}}a_j]\!]^{(\alpha\beta)} = 0 \text{ on } \partial Y^{(\alpha\beta)}, \tag{3.11}$$

$$\left\langle a_j^{(\alpha)} \right\rangle = \delta_{\alpha j}\phi_\alpha, \tag{3.12}$$

$$\text{Periodicity.} \tag{3.13}$$

For terms corresponding to $\nabla\mathcal{U}_j$, we find a coupling between both closure variables $\mathbf{b}_j^{(\alpha)}$ and $a_j^{(\alpha)}$ that stems from derivatives of the product $a_j^{(\alpha)}\mathcal{U}_j$. This yields

$$\widetilde{\mathcal{L}}^{(\alpha)}\mathbf{b}_j^{(\alpha)} = -\widetilde{\boldsymbol{\mathcal{J}}}^{(\alpha)}a_j^{(\alpha)} + \widetilde{\nabla} \cdot \left(\mathbf{A}^{(\alpha)}a_j^{(\alpha)}\right) \tag{3.14}$$

with

$$[\![\mathbf{b}_j]\!]^{(\alpha\beta)} = 0 \text{ on } \partial Y^{(\alpha\beta)}, \tag{3.15}$$

$$\mathbf{n}^{(\alpha\beta)} \cdot [\![\boldsymbol{\mathcal{J}}\mathbf{b}_j]\!]^{(\alpha\beta)} = \mathbf{n}^{(\alpha\beta)} \cdot [\![\mathbf{A}a_j]\!]^{(\alpha\beta)} \text{ on } \partial Y^{(\alpha\beta)}, \tag{3.16}$$

$$\left\langle \mathbf{b}_j^{(\alpha)} \right\rangle = 0, \tag{3.17}$$

$$\text{Periodicity,} \tag{3.18}$$

where we have used a perturbation notation generalized to operators, e.g.,

$$\widetilde{\boldsymbol{\mathcal{J}}}^{(\alpha)}a_j^{(\alpha)} = \boldsymbol{\mathcal{J}}^{(\alpha)}a_j^{(\alpha)} - \phi_\alpha^{-1}\left\langle \boldsymbol{\mathcal{J}}^{(\alpha)}a_j^{(\alpha)} \right\rangle. \tag{3.19}$$

Also, note the following important properties of the closure problems:

1. In the first set of closure problems, the equality $\sum_j a_j^{(\alpha)} = 1$ can be easily obtained by summing up all the different closure problems.
2. In the second set of closure problems, if $\mathbf{A}$ is continuous, then $\mathbf{n}^{(\alpha\beta)} \cdot [\![\mathbf{A} a_j]\!]^{(\alpha\beta)} = 0$.

Formally, we can condense these equations as

(3.20)
$$\begin{pmatrix} u^{(1)} \\ \vdots \\ u^{(N)} \end{pmatrix} = \begin{pmatrix} a_1^{(1)} & \cdots & a_N^{(1)} \\ \vdots & \ddots & \vdots \\ a_1^{(N)} & \cdots & a_N^{(N)} \end{pmatrix} \begin{pmatrix} \mathcal{U}_1 \\ \vdots \\ \mathcal{U}_N \end{pmatrix} + \begin{pmatrix} \mathbf{b}_1^{(1)} & \cdots & \mathbf{b}_N^{(1)} \\ \vdots & \ddots & \vdots \\ \mathbf{b}_1^{(N)} & \cdots & \mathbf{b}_N^{(N)} \end{pmatrix} \cdot \begin{pmatrix} \boldsymbol{\nabla}\mathcal{U}_1 \\ \vdots \\ \boldsymbol{\nabla}\mathcal{U}_N \end{pmatrix}$$

and the closure problems as

(3.21)
$$\begin{pmatrix} \widetilde{\mathcal{L}}^{(1)} & & \\ & \ddots & \\ & & \widetilde{\mathcal{L}}^{(N)} \end{pmatrix} \begin{pmatrix} a_1^{(1)} & \cdots & a_N^{(1)} \\ \vdots & \ddots & \vdots \\ a_1^{(N)} & \cdots & a_N^{(N)} \end{pmatrix} = 0,$$

(3.22)
$$\begin{pmatrix} \widetilde{\mathcal{L}}^{(1)} & & \\ & \ddots & \\ & & \widetilde{\mathcal{L}}^{(N)} \end{pmatrix} \begin{pmatrix} \mathbf{b}_1^{(1)} & \cdots & \mathbf{b}_N^{(1)} \\ \vdots & \ddots & \vdots \\ \mathbf{b}_1^{(N)} & \cdots & \mathbf{b}_N^{(N)} \end{pmatrix}$$
$$= \begin{pmatrix} -\widetilde{\boldsymbol{\mathcal{I}}}^{(1)} a_1^{(1)} + \widetilde{\nabla} \cdot \left(\mathbf{A}^{(1)} a_1^{(1)}\right) & \cdots & -\widetilde{\boldsymbol{\mathcal{I}}}^{(1)} a_N^{(1)} + \widetilde{\nabla} \cdot \left(\mathbf{A}^{(1)} a_N^{(1)}\right) \\ \vdots & \ddots & \vdots \\ -\widetilde{\boldsymbol{\mathcal{I}}}^{(N)} a_1^{(N)} + \widetilde{\nabla} \cdot \left(\mathbf{A}^{(N)} a_1^{(N)}\right) & \cdots & -\widetilde{\boldsymbol{\mathcal{I}}}^{(N)} a_N^{(N)} + \widetilde{\nabla} \cdot \left(\mathbf{A}^{(N)} a_N^{(N)}\right) \end{pmatrix},$$

with the same boundary and integral conditions. In this system, each line corresponds to a subdomain α while columns correspond to the source terms $\mathcal{U}_j$ and $\nabla\mathcal{U}_j$.

3.4. Eliminating integro-differential operators in the closure problems. The operator $\widetilde{\mathcal{L}}^{(\alpha)}\diamondsuit = \mathcal{L}^{(\alpha)}\diamondsuit - \phi_\alpha^{-1} \left\langle \mathcal{L}^{(\alpha)}\diamondsuit \right\rangle$ is, by definition, integro-differential with $\mathcal{L}^{(\alpha)}\diamondsuit$ partial differential and $\left\langle \mathcal{L}^{(\alpha)}\diamondsuit \right\rangle$ integral. However, $\left\langle \mathcal{L}^{(\alpha)}\diamondsuit \right\rangle$ is uniformly constant over each unit-cell because of the periodic boundary conditions. We can therefore eliminate the integral part of the operator using simple changes of the unknown functions.

3.4.1. First closure problem. The first closure problem can be written as a function of the coefficients $h_{\alpha j} \equiv \langle \mathcal{L}^{(\alpha)} a_j^{(\alpha)} \rangle$. Equation (3.21) reads

(3.23)
$$\begin{pmatrix} \mathcal{L}^{(1)} & & \\ & \ddots & \\ & & \mathcal{L}^{(N)} \end{pmatrix} \begin{pmatrix} a_1^{(1)} & \cdots & a_N^{(1)} \\ \vdots & \ddots & \vdots \\ a_1^{(N)} & \cdots & a_N^{(N)} \end{pmatrix} = \begin{pmatrix} \phi_1^{-1} & & \\ & \ddots & \\ & & \phi_N^{-1} \end{pmatrix} \begin{pmatrix} h_{11} & \cdots & h_{1N} \\ \vdots & \ddots & \vdots \\ h_{N1} & \cdots & h_{NN} \end{pmatrix},$$

with boundary conditions on $\partial Y^{(\alpha\beta)}$

$$[\![a_j]\!]^{(\alpha\beta)} = 0, \tag{3.24}$$

$$\mathbf{n}^{(\alpha\beta)} \cdot [\![\boldsymbol{\mathcal{J}} a_j]\!]^{(\alpha\beta)} = 0, \tag{3.25}$$

$$\left\langle a_j^{(\alpha)} \right\rangle = \phi_\alpha \delta_{\alpha j}, \tag{3.26}$$

$$\text{Periodicity.} \tag{3.27}$$

All the constant terms $h_{\alpha j}$ are not independent and before going on with the changes of unknown functions, we first need to make explicit the relationships between $h_{\alpha j}$. Considering the sum

$$\sum_{\alpha=1}^{N} h_{\alpha j} = \sum_{\alpha=1}^{N} \left\langle \mathcal{L}^{(\alpha)} a_j^{(\alpha)} \right\rangle = \sum_{\alpha=1}^{N} \left\langle \nabla \cdot \mathcal{J}^{(\alpha)} a_j^{(\alpha)} \right\rangle \tag{3.28}$$

and using the divergence theorem, it is straightforward that $\sum_{\alpha=1}^{N} h_{\alpha j} = 0$ because of the continuity of the fluxes between the different subdomains and the periodic boundary conditions. Therefore, we can write $h_{1j} = -\sum_{\alpha=2}^{N} h_{\alpha j}$ and

$$\begin{pmatrix} h_{11} & \cdots & h_{1N} \\ \vdots & \ddots & \vdots \\ h_{N1} & \cdots & h_{NN} \end{pmatrix} = \begin{pmatrix} -\sum_{\alpha=2}^{N} h_{\alpha 1} & \cdots & -\sum_{\alpha=2}^{N} h_{\alpha N} \\ h_{21} & \cdots & h_{2N} \\ \vdots & \ddots & \vdots \\ h_{N1} & \cdots & h_{NN} \end{pmatrix}. \tag{3.29}$$

With $(N-1) \times N$ unknowns for $h_{\alpha j}$, we now introduce the following decomposition:

$$\begin{pmatrix} a_1^{(1)} - 1 & \cdots & a_N^{(1)} \\ \vdots & \ddots & \vdots \\ a_1^{(N)} - 1 & \cdots & a_N^{(N)} \end{pmatrix} = \begin{pmatrix} d_2^{(1)} & \cdots & d_N^{(1)} \\ \vdots & \ddots & \vdots \\ d_2^{(N)} & \cdots & d_N^{(N)} \end{pmatrix} \begin{pmatrix} h_{21} & \cdots & h_{2N} \\ \vdots & \ddots & \vdots \\ h_{N1} & \cdots & h_{NN} \end{pmatrix}. \tag{3.30}$$

Further injecting (3.30) into (3.23), we have that $d_j^{(\alpha)}$ solves

$$\begin{pmatrix} \mathcal{L}^{(1)} & & \\ & \ddots & \\ & & \mathcal{L}^{(N)} \end{pmatrix} \begin{pmatrix} d_2^{(1)} & \cdots & d_N^{(1)} \\ \vdots & \ddots & \vdots \\ d_2^{(N)} & \cdots & d_N^{(N)} \end{pmatrix} = \begin{pmatrix} -\phi_1^{-1} & \cdots & -\phi_1^{-1} \\ \phi_2^{-1} & & \\ & \ddots & \\ & & \phi_N^{-1} \end{pmatrix} \tag{3.31}$$

with boundary conditions for $d_j^{(\alpha)}$ that are unchanged compared to $a_j^{(\alpha)}$, i.e., continuity inside the unit-cell and periodicity on the outside boundaries. Since integral terms have been removed and the problem is now purely differential on $d_j^{(\alpha)}$, this can be solved by standard numerical methods.

However, the values of $h_{\alpha j}$ are still unknown and to calculate them we need to consider the average conditions. For each column in (3.31), the variables $d_j^{(\alpha)}$ are defined uniquely up to a constant (see section 3.4.3 for details about existence and uniqueness) so that we must use an average condition to have a unique solution. We choose the average conditions $\langle d_j^{(1)} \rangle = 0$ to fix this constant. This choice is compatible with the average conditions applying to $a_j^{(1)}$, as we have from averaging the first line

in (3.30) that $\langle a_j^{(1)} \rangle = \phi_1 \delta_{1j}$. The rest of the average conditions on $a_j^{(\alpha>1)}$, i.e., $\langle a_j^{(\alpha)} \rangle = \phi_\alpha \delta_{\alpha j}$, are then used to calculate the exchange coefficients. Averaging (3.30) and removing the first line, which has already been used, we find the relationship

$$\begin{pmatrix} h_{22} & \cdots & h_{2N} \\ \vdots & \ddots & \vdots \\ h_{N2} & \cdots & h_{NN} \end{pmatrix} = \begin{pmatrix} \left\langle d_2^{(2)} \right\rangle & \cdots & \left\langle d_N^{(2)} \right\rangle \\ \vdots & \ddots & \vdots \\ \left\langle d_2^{(N)} \right\rangle & \cdots & \left\langle d_N^{(N)} \right\rangle \end{pmatrix}^{-1} \begin{pmatrix} \phi_2 & & \\ & \ddots & \\ & & \phi_N \end{pmatrix}, \tag{3.32}$$

which can be used to calculate the N^2 exchange coefficients $h_{\alpha j}$ when combined with $h_{1j} = -\sum_{\alpha=2}^{N} h_{\alpha j}$ and $h_{\alpha 1} = -\sum_{j=2}^{N} h_{\alpha j}$.

3.4.2. Second closure problem. We proceed in a similar way for the second closure problem. This may be written as

$$\begin{aligned} &\begin{pmatrix} \mathcal{L}^{(1)} & & \\ & \ddots & \\ & & \mathcal{L}^{(N)} \end{pmatrix} \begin{pmatrix} \mathbf{b}_1^{(1)} & \cdots & \mathbf{b}_N^{(1)} \\ \vdots & \ddots & \vdots \\ \mathbf{b}_1^{(N)} & \cdots & \mathbf{b}_N^{(N)} \end{pmatrix} \\ &= \begin{pmatrix} \phi_1^{-1} & & \\ & \ddots & \\ & & \phi_N^{-1} \end{pmatrix} \begin{pmatrix} \mathbf{V}_{11} & \cdots & \mathbf{V}_{1N} \\ \vdots & \ddots & \vdots \\ \mathbf{V}_{N1} & \cdots & \mathbf{V}_{NN} \end{pmatrix} \\ &\quad + \begin{pmatrix} -\widetilde{\boldsymbol{\mathcal{J}}}^{(1)} a_1^{(1)} + \widetilde{\nabla} \cdot \left(\mathbf{A}^{(1)} a_1^{(1)} \right) & \cdots & -\widetilde{\boldsymbol{\mathcal{J}}}^{(1)} a_N^{(1)} + \widetilde{\nabla} \cdot \left(\mathbf{A}^{(1)} a_N^{(1)} \right) \\ \vdots & \ddots & \vdots \\ -\widetilde{\boldsymbol{\mathcal{J}}}^{(N)} a_1^{(N)} + \widetilde{\nabla} \cdot \left(\mathbf{A}^{(N)} a_1^{(N)} \right) & \cdots & -\widetilde{\boldsymbol{\mathcal{J}}}^{(N)} a_N^{(N)} + \widetilde{\nabla} \cdot \left(\mathbf{A}^{(N)} a_N^{(N)} \right) \end{pmatrix} \end{aligned} \tag{3.33}$$

with

$$\mathbf{V}_{\alpha j} = \left\langle \mathcal{L}^{(\alpha)} \mathbf{b}_j^{(\alpha)} \right\rangle. \tag{3.34}$$

We use the following change of unknown functions:

$$\begin{aligned} \begin{pmatrix} \mathbf{b}_1^{(1)} & \cdots & \mathbf{b}_N^{(1)} \\ \vdots & \ddots & \vdots \\ \mathbf{b}_1^{(N)} & \cdots & \mathbf{b}_N^{(N)} \end{pmatrix} &= \begin{pmatrix} \mathbf{e}_1^{(1)} & \cdots & \mathbf{e}_N^{(1)} \\ \vdots & \ddots & \vdots \\ \mathbf{e}_1^{(N)} & \cdots & \mathbf{e}_N^{(N)} \end{pmatrix} \\ &\quad + \begin{pmatrix} d_2^{(1)} & \cdots & d_N^{(1)} \\ \vdots & \ddots & \vdots \\ d_2^{(N)} & \cdots & d_N^{(N)} \end{pmatrix} \begin{pmatrix} \mathbf{V}_{21} & \cdots & \mathbf{V}_{2N} \\ \vdots & \ddots & \vdots \\ \mathbf{V}_{N1} & \cdots & \mathbf{V}_{NN} \end{pmatrix}. \end{aligned} \tag{3.35}$$

The idea here is to use the linearity of the operators in order to decompose the solution into two distinct parts corresponding to different source terms in the equations. Here, $\mathbf{e}_j^{(\alpha)}$ are solutions of

$$\begin{pmatrix} \mathcal{L}^{(1)} & & \\ & \ddots & \\ & & \mathcal{L}^{(N)} \end{pmatrix} \begin{pmatrix} \mathbf{e}_1^{(1)} & \cdots & \mathbf{e}_N^{(1)} \\ \vdots & \ddots & \vdots \\ \mathbf{e}_1^{(N)} & \cdots & \mathbf{e}_N^{(N)} \end{pmatrix} = \widetilde{\mathbb{S}} \tag{3.36}$$

with the average condition $\langle \mathbf{e}_j^{(1)} \rangle = 0$, continuity/jump conditions on boundaries, and

$$\widetilde{\mathbb{S}} = \begin{pmatrix} -\widetilde{\boldsymbol{\mathcal{J}}}^{(1)} a_1^{(1)} + \widetilde{\nabla} \cdot \left(\mathbf{A}^{(1)} a_1^{(1)} \right) & \cdots & -\widetilde{\boldsymbol{\mathcal{J}}}^{(1)} a_N^{(1)} + \widetilde{\nabla} \cdot \left(\mathbf{A}^{(1)} a_N^{(1)} \right) \\ \vdots & \ddots & \vdots \\ -\widetilde{\boldsymbol{\mathcal{J}}}^{(N)} a_1^{(N)} + \widetilde{\nabla} \cdot \left(\mathbf{A}^{(N)} a_1^{(N)} \right) & \cdots & -\widetilde{\boldsymbol{\mathcal{J}}}^{(N)} a_N^{(N)} + \widetilde{\nabla} \cdot \left(\mathbf{A}^{(N)} a_N^{(N)} \right) \end{pmatrix}. \tag{3.37}$$

$\mathbf{V}_{\alpha j}$ can then be calculated by averaging (3.35) and removing the first line to obtain

$$\begin{pmatrix} \mathbf{V}_{21} & \cdots & \mathbf{V}_{2N} \\ \vdots & \ddots & \vdots \\ \mathbf{V}_{N1} & \cdots & \mathbf{V}_{NN} \end{pmatrix} = - \begin{pmatrix} \left\langle d_2^{(2)} \right\rangle & \cdots & \left\langle d_N^{(2)} \right\rangle \\ \vdots & \ddots & \vdots \\ \left\langle d_2^{(N)} \right\rangle & \cdots & \left\langle d_N^{(N)} \right\rangle \end{pmatrix}^{-1} \begin{pmatrix} \left\langle \mathbf{e}_1^{(2)} \right\rangle & \cdots & \left\langle \mathbf{e}_N^{(2)} \right\rangle \\ \vdots & \ddots & \vdots \\ \left\langle \mathbf{e}_1^{(N)} \right\rangle & \cdots & \left\langle \mathbf{e}_N^{(N)} \right\rangle \end{pmatrix}, \tag{3.38}$$

or equivalently, combined with (3.32), we also have

$$\begin{pmatrix} \mathbf{V}_{11} & \cdots & \mathbf{V}_{1N} \\ \vdots & \ddots & \vdots \\ \mathbf{V}_{N1} & \cdots & \mathbf{V}_{NN} \end{pmatrix} = - \begin{pmatrix} h_{11} & \cdots & h_{1N} \\ \vdots & \ddots & \vdots \\ h_{N1} & \cdots & h_{NN} \end{pmatrix} \begin{pmatrix} \phi_1^{-1} & & \\ & \ddots & \\ & & \phi_N^{-1} \end{pmatrix} \begin{pmatrix} \left\langle \mathbf{e}_1^{(1)} \right\rangle & \cdots & \left\langle \mathbf{e}_N^{(1)} \right\rangle \\ \vdots & \ddots & \vdots \\ \left\langle \mathbf{e}_1^{(N)} \right\rangle & \cdots & \left\langle \mathbf{e}_N^{(N)} \right\rangle \end{pmatrix}. \tag{3.39}$$

3.4.3. Solvability condition for the closure problems. The closure problems (3.31) and (3.36) are not homogeneous. Because of the periodic boundary condition, there are strong constraints applying to the source terms on the right-hand sides of these equations. Classical results of the analysis of elliptic equations show that these problems are well-posed under the solvability condition:

$$\int_Y \mathcal{S}_j = 0. \tag{3.40}$$

We can easily check that this is true for all the source terms in the closure problems. For d_j, we have $\mathcal{S}_j^d = -\phi_1^{-1}\chi^{(1)} + \phi_j^{-1}\chi^{(j)}$, for which it is trivial to show that $\int_Y \mathcal{S}_j^d = 0$. In the other closure problem, (3.36), the source terms, $\widetilde{\mathbb{S}}$, are perturbations in the form $\mathcal{S}_j^{\mathcal{M}} = \sum_\alpha [\chi^{(\alpha)} \mathcal{M}_j^{(\alpha)} - \int_Y \chi^{(\alpha)} \mathcal{M}_j^{(\alpha)}]$ that also verify $\int_Y \mathcal{S}_j^{\mathcal{M}} = 0$.

3.5. Average model. Equation (3.1) can be written as, for any point in Ω,

$$\phi_\alpha \partial_t \mathcal{U}_\alpha + \left\langle \nabla \cdot \boldsymbol{\mathcal{J}}^{(\alpha)} u^{(\alpha)} \right\rangle = 0. \tag{3.41}$$

3.5.1. Complete model. Injecting (3.8) into (3.41), we obtain

$$\phi_\alpha \partial_t \mathcal{U}_\alpha + \mathbf{C}_{\alpha j} \cdot \boldsymbol{\nabla} \mathcal{U}_j = \mathbf{A}_{\alpha j} : \boldsymbol{\nabla}\boldsymbol{\nabla} \mathcal{U}_j - h_{\alpha j} \mathcal{U}_j \tag{3.42}$$

with exchange coefficients

$$h_{\alpha j} = \left\langle \mathcal{L}^{(\alpha)} a_j^{(\alpha)} \right\rangle, \tag{3.43}$$

effective velocities

$$\mathbf{C}_{\alpha j} = \left\langle \mathcal{L}^{(\alpha)} \mathbf{b}_j^{(\alpha)} \right\rangle - \left\langle \nabla \cdot \left(\mathbf{A}^{(\alpha)} a_j^{(\alpha)} \right) \right\rangle + \left\langle \boldsymbol{\mathcal{J}}^{(\alpha)} a_j^{(\alpha)} \right\rangle, \tag{3.44}$$

and dispersion tensors

$$\mathbf{A}_{\alpha j} = \left\langle \mathbf{A}^{(\alpha)} a_j^{(\alpha)} \right\rangle - \left\langle \boldsymbol{\mathcal{J}}^{(\alpha)} \mathbf{b}_j^{(\alpha)} \right\rangle. \tag{3.45}$$

This problem can be written formally as

$$\partial_t \begin{pmatrix} \phi_1 \mathcal{U}_1 \\ \vdots \\ \phi_N \mathcal{U}_N \end{pmatrix} + \mathbb{C}_N \cdot \begin{pmatrix} \boldsymbol{\nabla} \mathcal{U}_1 \\ \vdots \\ \boldsymbol{\nabla} \mathcal{U}_N \end{pmatrix} = \mathbb{A}_N : \begin{pmatrix} \boldsymbol{\nabla}\boldsymbol{\nabla} \mathcal{U}_1 \\ \vdots \\ \boldsymbol{\nabla}\boldsymbol{\nabla} \mathcal{U}_N \end{pmatrix} - \begin{pmatrix} h_{11} & \cdots & h_{1N} \\ \vdots & \ddots & \vdots \\ h_{N1} & \cdots & h_{NN} \end{pmatrix} \begin{pmatrix} \mathcal{U}_1 \\ \vdots \\ \mathcal{U}_N \end{pmatrix} \tag{3.46}$$

with

$$\mathbb{C}_N = \begin{pmatrix} \mathbf{C}_{11} & \cdots & \mathbf{C}_{1N} \\ \vdots & \ddots & \vdots \\ \mathbf{C}_{N1} & \cdots & \mathbf{C}_{NN} \end{pmatrix} \quad \text{and} \quad \mathbb{A}_N = \begin{pmatrix} \mathbf{A}_{11} & \cdots & \mathbf{A}_{1N} \\ \vdots & \ddots & \vdots \\ \mathbf{A}_{N1} & \cdots & \mathbf{A}_{NN} \end{pmatrix}. \tag{3.47}$$

Since we consider a homogeneous porous medium here, we can also write this in a conservative form as

$$\partial_t \begin{pmatrix} \phi_1 \mathcal{U}_1 \\ \vdots \\ \phi_N \mathcal{U}_N \end{pmatrix} + \boldsymbol{\nabla} \cdot \left[\mathbb{C}_N \begin{pmatrix} \mathcal{U}_1 \\ \vdots \\ \mathcal{U}_N \end{pmatrix} \right] = \boldsymbol{\nabla} \cdot \left[\mathbb{A}_N \cdot \begin{pmatrix} \boldsymbol{\nabla} \mathcal{U}_1 \\ \vdots \\ \boldsymbol{\nabla} \mathcal{U}_N \end{pmatrix} \right] - \begin{pmatrix} h_{11} & \cdots & h_{1N} \\ \vdots & \ddots & \vdots \\ h_{N1} & \cdots & h_{NN} \end{pmatrix} \begin{pmatrix} \mathcal{U}_1 \\ \vdots \\ \mathcal{U}_N \end{pmatrix}. \tag{3.48}$$

3.5.2. Discussion. Problem (3.48) is a system of convection-diffusion-reaction equations with constant coefficients, so that standard results of partial derivative equations analysis show that it admits a unique global in time solution as soon as the diffusion matrix $\mathbb{A}_N$ satisfies the coercivity assumption $\xi^t \mathbb{A}_N \xi > \alpha |\xi|^2$ for any vector ξ of $\mathbb{R}^{N \times n}$ with $\alpha > 0$ (see, e.g., [11, pp. 340–341] and references therein). Thus far, we have not been able to prove this property for the general expression of matrices $\mathbb{A}_N$ given in terms of the closure problems. However, since $\mathbb{A}_N$ is a constant real matrix, it may be checked a posteriori each time for the specific problem at hand. With this respect, note that $\mathbb{A}_N$ may be replaced in the coercivity relation by its symmetric part $1/2(\mathbb{A}_N + \mathbb{A}_N^t)$, which is diagonalizable. In practice, the issue of coercivity thus boils down to searching for the lowest eigenvalue of a symmetric real matrix, and many packages are available for this purpose.

Independently from the issue of well-posedness, the nondiagonal terms in $\mathbb{C}_N$ and $\mathbb{A}_N$ may yield unphysical results, such as negative concentrations or values outside

initial bounds (see an example in section 4.5). Physically, these issues stem from the fact that the derivation of the model above, (3.46), is based on a particular form of the solution (3.7) and a set of hypotheses that may not be correct for any initial/boundary condition or any point in the domain. The result is that the macroscale model may yield negative concentrations, so that the model needs to be used carefully. Some of the hypotheses used in deriving the closure (3.7) may not always be valid and examples for which the model yields nonphysical results can be easily constructed for specific choices of initial conditions (see an example in section 4.5).

The question of coercivity is a major one, as it conditions the well-posedness of the problem. In practical applications, if the coercivity is not verified, regularization is one way to resolve the issue. For instance, one may use an approximant of $\mathbb{A}_N$ that has all the required properties to obtain a well-posed problem, e.g., the nearest symmetric positive semidefinite matrix to $\mathbb{A}_N$ [28], possibly constrained to respect important properties, such as to keep the sum of all the terms $\sum_{i,j} \mathbf{A}_{ij}$ identical. In the one-dimensional numerical examples treated in section 4, there is no need for such elaborate approaches as the coercivity of the matrix was obtained for all the cases presented. However, we emphasize that this needs to be dealt with carefully and that either a demonstration of general coercivity or a robust approach to correct it will be needed for the general case.

The issue about respecting initial bounds is not as important as, in many cases, the primary goal is to obtain an accurate approximation of the signal, even if it means breaking min/max principles. This problem is not specific to the VAT but rather stems from the multirate macroscopic formulation and was already observed in [22]. In many cases, obtaining a slightly negative concentration may be acceptable especially if this vanishes in the long-time limit [22]. In section 4.5, we provide examples of negative solutions that still capture all the important features of the scalar field. If this cannot be tolerated for a particular problem, a variety of approaches could be used. As a very simple example, we can diagonalize the velocity and dispersion matrices via lumping as

(3.49)
$$\begin{pmatrix} \mathbf{C}_{11} & \cdots & \mathbf{C}_{1N} \\ \vdots & \ddots & \vdots \\ \mathbf{C}_{N1} & \cdots & \mathbf{C}_{NN} \end{pmatrix} \to \begin{pmatrix} \mathbf{C}_1 & & \\ & \ddots & \\ & & \mathbf{C}_N \end{pmatrix} \quad \text{and} \quad \begin{pmatrix} \mathbf{A}_{11} & \cdots & \mathbf{A}_{1N} \\ \vdots & \ddots & \vdots \\ \mathbf{A}_{N1} & \cdots & \mathbf{A}_{NN} \end{pmatrix} \to \begin{pmatrix} \phi_1 \mathbf{A}^* & & \\ & \ddots & \\ & & \phi_N \mathbf{A}^* \end{pmatrix}$$

with $\mathbf{C}_\alpha = \sum_j \mathbf{C}_{\alpha j}$ and $\mathbf{A}^* = \sum_{\alpha,j} \mathbf{A}_{ij}$. Example solutions with this simplification are presented in section 4.5. Another approach could be to weight nondiagonal terms with a regularizing function that eliminates the nondiagonal terms when $\mathcal{U}_j$ is getting close to initial bounds (zero, for example). Similar approaches are used for diffusion reaction models with cross-diffusion in biological systems [51] or multicomponent mass transport [49, 24]. A considerable issue, however, is that the system becomes nonlinear, making computations of the solutions a lot more complicated.

3.5.3. Theoretical comparison with MRMT. How is this model different from MRMT? Besides the fact that, contrary to MRMT models, we have derived a direct link (the closure problems) between the microscale geometry and the effective parameters, there are also differences in the macroscale form compared to MRMT models. To better understand this, we consider the generic form from [4] that we straightforwardly extend to the mobile-mobile cases by allowing each phase to flow. With our formalism, this reads

(3.50)
$$\partial_t \begin{pmatrix} \phi_1 \mathcal{U}_1 \\ \vdots \\ \phi_N \mathcal{U}_N \end{pmatrix} + \boldsymbol{\nabla}\cdot \left[\mathbb{Q}_N \begin{pmatrix} \mathcal{U}_1 \\ \vdots \\ \mathcal{U}_N \end{pmatrix} \right] = \boldsymbol{\nabla}\cdot \left[\mathbb{D}_N \cdot \begin{pmatrix} \boldsymbol{\nabla}\mathcal{U}_1 \\ \vdots \\ \boldsymbol{\nabla}\mathcal{U}_N \end{pmatrix} \right] - \begin{pmatrix} h_{11} & \cdots & h_{1N} \\ \vdots & \ddots & \vdots \\ h_{N1} & \cdots & h_{NN} \end{pmatrix} \begin{pmatrix} \mathcal{U}_1 \\ \vdots \\ \mathcal{U}_N \end{pmatrix}$$

with

$$\mathbb{Q}_N = \begin{pmatrix} \langle \mathbf{v}^{(1)} \rangle & & \\ & \ddots & \\ & & \langle \mathbf{v}^{(N)} \rangle \end{pmatrix} \quad \text{and} \quad \mathbb{D}_N = \begin{pmatrix} \phi_1 d_1 & & \\ & \ddots & \\ & & \phi_N d_N \end{pmatrix}. \tag{3.51}$$

The first striking difference is that $\mathbb{C}_N$ and $\mathbb{A}_N$ feature nondiagonal (coupling) terms, whereas the MRMT model does not. From a theoretical point of view, this suggests that the model derived here is actually more general as it contains additional couplings. The simplified diagonalized version of our model with (3.49) is almost identical to the MRMT. The only difference is that the values of the terms on the diagonal are not necessarily the same. The most obvious example of this is for the velocities. Indeed, for $\mathbb{Q}_N$ the diagonal terms correspond to the average physical velocity of each subdomain, whereas $\mathbf{C}_\alpha$ contains additional terms.

4. Validation against direct numerical simulations.

4.1. Description of the geometries and microscale problems. As a toy problem, we consider scalar transport in two-dimensional periodic arrays of 40 unit-cells (see Figure 4.1(a)). Each unit-cell (see Figure 4.1(b)–(f)) consists of a fluid phase f with incompressible Stokes flow (see solutions for individual unit-cells in Figure 4.1(g)–(i)),

$$0 = -\nabla p + \mu \Delta \mathbf{v} + \mathbf{e}_x \text{ in phase } f, \tag{4.1}$$

$$\nabla \cdot \mathbf{v} = 0 \text{ in phase } f, \tag{4.2}$$

$$\mathbf{v} = 0 \text{ on } \partial\Omega_t, \, \partial\Omega_b, \text{ and } \partial\Omega_{fn_i}, \tag{4.3}$$

$$\text{Periodicity on } \partial\Omega_l \text{ and } \partial\Omega_r. \tag{4.4}$$

For the scalar transport problem, we have

$$\partial_t u^{(f)} + \mathbf{v} \cdot \nabla u^{(f)} = \frac{1}{\mathrm{Pe}} \Delta u^{(f)} \text{ in phase } f, \tag{4.5}$$

$$\partial_t u^{(n_i)} = \frac{\Gamma^{(n_i)}}{\mathrm{Pe}} \Delta u^{(n_i)} \text{ in the nodule } n_i, \tag{4.6}$$

$$u^{(f)} = u^{(n_i)} \text{ on } \partial\Omega_{fn_i}, \tag{4.7}$$

$$\mathbf{n}_{fn_i} \cdot \nabla u^{(f)} = \mathbf{n}_{fn_i} \cdot \Gamma^{(n_i)} \nabla u^{(n_i)} \text{ on } \partial\Omega_{fn_i}, \tag{4.8}$$

$$\partial_y u = 0 \text{ on } \partial\Omega_t \text{ and } \partial\Omega_b, \tag{4.9}$$

$$u = 0 \text{ on } \partial\Omega_l \text{ and } \partial\Omega_r, \tag{4.10}$$

$$u\,(x, y, t = 0) = \frac{1}{\sigma\sqrt{2\pi}} e^{-\frac{(x-\mu)^2}{2\sigma^2}}. \tag{4.11}$$

We consider two classes of geometries for the unit-cell, one with a relatively large centered nodule and one with two smaller nodules (dashed line in Figure 4.1). We impose $\Gamma^{(n_\alpha)} = 1.0$ for the case with one nodule and $\Gamma^{(n_\beta)} = 0.1$, $\Gamma^{(n_\gamma)} = 0.01$ for the geometry with two nodules.

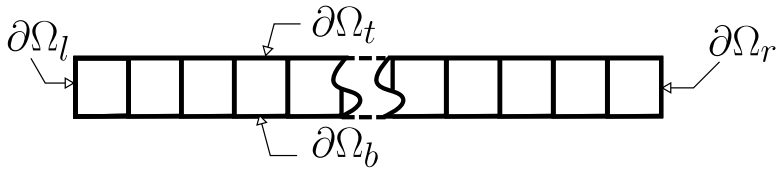

(a) Macroscopic geometry

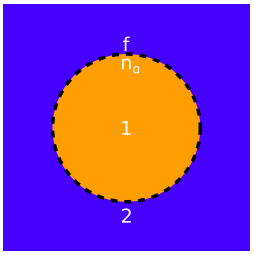

(b) 2 subdomains, center.

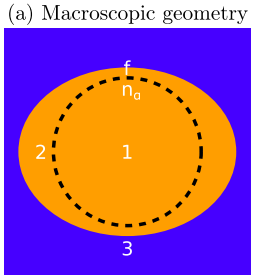

(c) 2 subdomains, ellipse.

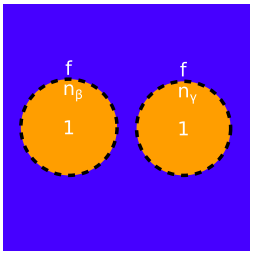

(d) 2 subdomains.

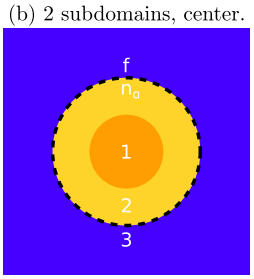

(e) 3 subdomains, center.

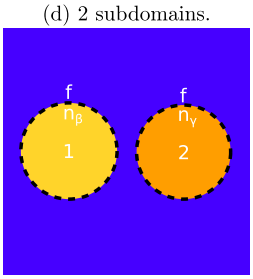

(f) 3 subdomains.

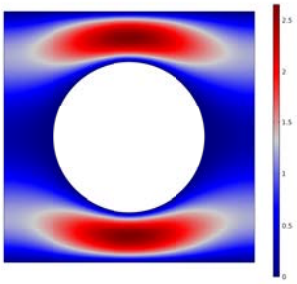

(g) velocity field, one nodule.

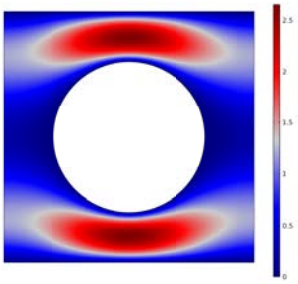

(h) velocity field, one nodule.

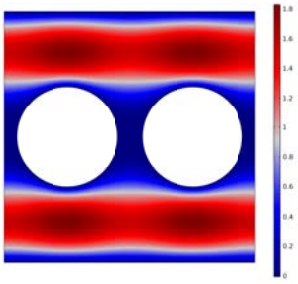

(i) velocity field, two nodules.

FIG. 4.1. *Geometries of* (a) *the whole domain containing a total of* 40 *unit-cells.* (b)–(f) *Geometries of each unit-cell with the one- and two-nodule configurations. The dashed lines correspond to the geometry while the colors describe the subdomain decomposition. The letters* f *and* n *refer to the decomposition for the microscale transport with, respectively, the fluid (*f*) and nodules (*n_α*,* n_β*,* n_γ*). The numbers* 1, 2, *and* 3 *correspond to the subdomain decomposition for the macroscale model, which is independent from the fluid/nodule decomposition.* (g)–(i) *The normalized* x*-component of the velocity field,* $\frac{v_x}{\phi_f^{-1}\langle v_x\rangle}$*, for one and two nodules.*

4.2. Macroscale problems. We consider the one-, two-, and three-equation models for each geometry (referred to as 1eq, 2eq, and 3eq). For 1eq, the macroscale problem reads

$$\partial_t \mathcal{U} + \langle v\rangle\, \partial_x \mathcal{U}^{1eq} = A^\star \partial_{xx} \mathcal{U}^{1eq} \tag{4.12}$$

with $A^\star$ the standard dispersion tensor (see [52, 45, 9]). For 2eq (Figure 4.1(b), (c), and (d)), we have

$$\begin{aligned}&\begin{pmatrix}\phi_1 & 0\\ 0 & \phi_2\end{pmatrix}\partial_t\begin{pmatrix}\mathcal{U}_1^{2eq}\\ \mathcal{U}_2^{2eq}\end{pmatrix}+\begin{pmatrix}C_{11} & C_{12}\\ C_{21} & C_{22}\end{pmatrix}\partial_x\begin{pmatrix}\mathcal{U}_1^{2eq}\\ \mathcal{U}_2^{2eq}\end{pmatrix}\\ &=\begin{pmatrix}A_{11} & A_{12}\\ A_{21} & A_{22}\end{pmatrix}\partial_{xx}\begin{pmatrix}\mathcal{U}_1^{2eq}\\ \mathcal{U}_2^{2eq}\end{pmatrix}-\begin{pmatrix}h_{11} & h_{12}\\ h_{21} & h_{22}\end{pmatrix}\begin{pmatrix}\mathcal{U}_1^{2eq}\\ \mathcal{U}_2^{2eq}\end{pmatrix},\end{aligned}\tag{4.13}$$

and finally, for the 3eq (Figure 4.1(e) and (f)),

$$\begin{aligned}&\begin{pmatrix}\phi_1 & 0 & 0\\ 0 & \phi_2 & 0\\ 0 & 0 & \phi_3\end{pmatrix}\partial_t\begin{pmatrix}\mathcal{U}_1^{3eq}\\ \mathcal{U}_2^{3eq}\\ \mathcal{U}_3^{3eq}\end{pmatrix}+\begin{pmatrix}C_{11} & C_{12} & C_{13}\\ C_{12} & C_{22} & C_{23}\\ C_{13} & C_{23} & C_{33}\end{pmatrix}\partial_x\begin{pmatrix}\mathcal{U}_1^{3eq}\\ \mathcal{U}_2^{3eq}\\ \mathcal{U}_3^{3eq}\end{pmatrix}\\ &=\begin{pmatrix}A_{11} & A_{12} & A_{13}\\ A_{12} & A_{22} & A_{23}\\ A_{13} & A_{23} & A_{33}\end{pmatrix}\partial_{xx}\begin{pmatrix}\mathcal{U}_1^{3eq}\\ \mathcal{U}_2^{3eq}\\ \mathcal{U}_3^{3eq}\end{pmatrix}-\begin{pmatrix}h_{11} & h_{12} & h_{13}\\ h_{21} & h_{22} & h_{23}\\ h_{31} & h_{32} & h_{33}\end{pmatrix}\begin{pmatrix}\mathcal{U}_1^{3eq}\\ \mathcal{U}_2^{3eq}\\ \mathcal{U}_3^{3eq}\end{pmatrix}.\end{aligned}\tag{4.14}$$

We also consider the simplified diagonalized equations (as described in section 3.5.2)

$$\begin{aligned}&\begin{pmatrix}\phi_1 & 0\\ 0 & \phi_2\end{pmatrix}\partial_t\begin{pmatrix}\mathcal{U}_1^{S2eq}\\ \mathcal{U}_2^{S2eq}\end{pmatrix}+\begin{pmatrix}C_1 & 0\\ 0 & C_2\end{pmatrix}\partial_x\begin{pmatrix}\mathcal{U}_1^{S2eq}\\ \mathcal{U}_2^{S2eq}\end{pmatrix}\\ &=\begin{pmatrix}\phi_1 A^{*2eq} & 0\\ 0 & \phi_2 A^{*2eq}\end{pmatrix}\partial_{xx}\begin{pmatrix}\mathcal{U}_1^{S2eq}\\ \mathcal{U}_2^{S2eq}\end{pmatrix}-\begin{pmatrix}h_{11} & h_{12}\\ h_{21} & h_{22}\end{pmatrix}\begin{pmatrix}\mathcal{U}_1^{S2eq}\\ \mathcal{U}_2^{S2eq}\end{pmatrix},\end{aligned}\tag{4.15}$$

and finally, for the 3eq,

$$\begin{aligned}&\begin{pmatrix}\phi_1 & 0 & 0\\ 0 & \phi_2 & 0\\ 0 & 0 & \phi_3\end{pmatrix}\partial_t\begin{pmatrix}\mathcal{U}_1^{S3eq}\\ \mathcal{U}_2^{S3eq}\\ \mathcal{U}_3^{S3eq}\end{pmatrix}+\begin{pmatrix}C_1 & 0 & 0\\ 0 & C_2 & 0\\ 0 & 0 & C_3\end{pmatrix}\partial_x\begin{pmatrix}\mathcal{U}_1^{S3eq}\\ \mathcal{U}_2^{s3eq}\\ \mathcal{U}_3^{S3eq}\end{pmatrix}\\ &=\begin{pmatrix}\phi_1 A^{*3eq} & 0 & 0\\ 0 & \phi_2 A^{*3eq} & 0\\ 0 & 0 & \phi_3 A^{*3eq}\end{pmatrix}\partial_{xx}\begin{pmatrix}\mathcal{U}_1^{S3eq}\\ \mathcal{U}_2^{S3eq}\\ \mathcal{U}_3^{S3eq}\end{pmatrix}-\begin{pmatrix}h_{11} & h_{12} & h_{13}\\ h_{21} & h_{22} & h_{23}\\ h_{31} & h_{32} & h_{33}\end{pmatrix}\begin{pmatrix}\mathcal{U}_1^{S3eq}\\ \mathcal{U}_2^{S3eq}\\ \mathcal{U}_3^{S3eq}\end{pmatrix}.\end{aligned}\tag{4.16}$$

For the initial condition, we impose $\mathcal{U}(x,t=0)=\frac{1}{\sigma\sqrt{2\pi}}e^{-\frac{(x-\mu)^2}{2\sigma^2}}$, for all models, this corresponding to the initial condition of the microscale model in section 4.1. For the boundary conditions, we have $\mathcal{U}(x=0,t)=0$ and $\mathcal{U}(x=40,t)=0$.

4.3. Numerical methods.

4.3.1. General description. Microscale (section 4.1) and macroscale (section 4.2) equations are solved using standard finite element methods. Stokes flow at the microscale is solved on a P2/P1 Lagrange basis. Microscale advection-diffusion equations for the direct numerical solution and the closure problems are solved on cubic Lagrange elements with streamline and crosswind diffusion. Macroscale equations are solved on quadratic Lagrange elements without stabilization. The time discretization for direct numerical simulations and the macroscale equations is implicit with the backward differentiation formula. For the resolution of linear systems, we use MUMPS (Multifrontal massively parallel sparse direct solver).

4.4. Resolution algorithm. First, we solve directly the microscale model (section 4.1), this serving as a reference for comparison with homogenized models. Second, we solve the homogenized problem with the different models. To do so, we start by solving the closure problems for d and e over each unit-cell with periodic boundary conditions (Figure 4.1, orange, yellow, and blue corresponding to different subdomains). We then use these fields to calculate the effective parameters and construct a and b (section 3.4) for each value of the Péclet number, Pe. For all cases presented, we verified that the dispersion matrices are coercive, so that the problems are well-posed. Once we have calculated the values of the effective parameters as functions of Pe, the macroscale models are solved to obtain $\mathcal{U}_i$ for one, two, and three subdomains (section 4.2). The accuracy of each homogenized model can then be evaluated by comparing these results to those obtained from the direct numerical simulations of the microscale model.

We will go one step further in the comparison by reconstructing the microscale fields from $\mathcal{U}_i$ and the closure fields a and b. The first step in doing so is to extend the fields a and b, only defined over a single unit-cell, to the entire domain by periodicity. The corrector-type results may then simply be written as

$$u^{1eq}(x,y,t) = \mathcal{U}^{1eq}(x,t) + b(x,y)\,\partial_x \mathcal{U}^{1eq}(x,t), \tag{4.17}$$

$$u^{2eq}(x,y,t) = \begin{pmatrix} a_1(x,y) \\ a_2(x,y) \end{pmatrix} \begin{pmatrix} \mathcal{U}_1^{2eq}(x,t) \\ \mathcal{U}_2^{2eq}(x,t) \end{pmatrix} + \begin{pmatrix} b_1(x,y) \\ b_2(x,y) \end{pmatrix} \begin{pmatrix} \partial_x \mathcal{U}_1^{2eq}(x,t) \\ \partial_x \mathcal{U}_2^{2eq}(x,t) \end{pmatrix}, \tag{4.18}$$

$$u^{3eq}(x,y,t) = \begin{pmatrix} a_1(x,y) \\ a_2(x,y) \\ a_3(x,y) \end{pmatrix} \begin{pmatrix} \mathcal{U}_1^{3eq}(x,t) \\ \mathcal{U}_2^{3eq}(x,t) \\ \mathcal{U}_3^{3eq}(x,t) \end{pmatrix} + \begin{pmatrix} b_1(x,y) \\ b_2(x,y) \\ b_3(x,y) \end{pmatrix} \begin{pmatrix} \partial_x \mathcal{U}_1^{3eq}(x,t) \\ \partial_x \mathcal{U}_2^{3eq}(x,t) \\ \partial_x \mathcal{U}_3^{3eq}(x,t) \end{pmatrix}, \tag{4.19}$$

which can be directly compared to direct numerical simulations of $u^{(f)}$ and $u^{(n_i)}$, that we simply write u^{dns} over the entire unit-cell.

4.5. Results and discussion. To facilitate comparison of the two-dimensional fields from direct numerical simulations, $u^{dns}(x,y,t)$, with the one-dimensional fields from the macroscale equations, we project $u^{dns}(x,y,t)$ onto the x-axis and define $u^{Pdns}(x,t) = \int_0^1 u^{dns}(x,y,t)\,dy$. Although $u^{Pdns}(x,t)$ still contains high-frequency fluctuations in x, it is one-dimensional and therefore can be easily compared to

$$\mathcal{U}^{Neq}(x,t) = \sum_i \phi_i \mathcal{U}_i^{Neq}(x,t)$$

for the one-equation, $\mathcal{U}^{1eq}$, two-equation, $\mathcal{U}^{2eq}$, and three-equation $\mathcal{U}^{3eq}$ models.

4.5.1. Preliminary aspects. In this first section, we present ancillary results regarding the effect of the initial condition, of matrix diagonalization, and of the choice of domain decomposition. These aspects are not fully explored here and only serve as a basis to understand and discuss the impact of the number of subdomains on the results, which is studied in the remainder of section 4.5.

We start by assessing the influence of the initial condition for the case with one nodule and Pe = 300. Figure 4.2 presents $\mathcal{U}_2^{3eq}$ and $\mathcal{U}_2^{S3eq}$ (geometry in Figure 4.1(e)) at time $t = 1$ for increasing values of the standard deviation, σ, of the initial Gaussian signal. Results show that the smallest value of σ, which corresponds to the strongest initial gradients of concentration, yields negative solutions for $\mathcal{U}_2^{3eq}$, as was already observed for MRMT in [22]. We also see that this effect disappears when the gradients occur over a lengthscale that is much larger than the unit-cell. This is because strong

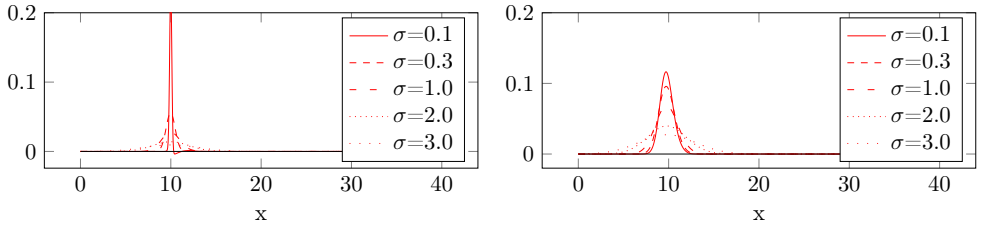

FIG. 4.2. *Comparisons (geometry in Figure* 4.1e*) of non-diagonalized* $\mathcal{U}_2^{3eq}$ *and diagonalized* $\mathcal{U}_2^{S3eq}$ *models (in subdomain* 2*) for different values* σ*, the standard deviation of the initial condition, and* ($Pe = 300$ *and* $t = 1$*).*

gradients are incompatible with assumptions in the VAT and, therefore, may lead to unphysical results of the model. To understand this, let us construct a simple example showing analytically how a two-domain decomposition can lead to negative solutions. We consider

$$\partial_t \begin{pmatrix} \phi_1 \mathcal{U}_1 \\ \phi_2 \mathcal{U}_2 \end{pmatrix} + \begin{pmatrix} C_{11} & C_{12} \\ C_{21} & C_{22} \end{pmatrix} \begin{pmatrix} \partial_x \mathcal{U}_1 \\ \partial_x \mathcal{U}_2 \end{pmatrix} = \begin{pmatrix} \mathsf{A}_{11} & \mathsf{A}_{12} \\ \mathsf{A}_{21} & \mathsf{A}_{22} \end{pmatrix} \begin{pmatrix} \partial_{xx} \mathcal{U}_1 \\ \partial_{xx} \mathcal{U}_2 \end{pmatrix} - \begin{pmatrix} h_{11} & h_{12} \\ h_{21} & h_{22} \end{pmatrix} \begin{pmatrix} \mathcal{U}_1 \\ \mathcal{U}_2 \end{pmatrix} \tag{4.20}$$

on $\mathbb{R} \times \mathbb{R}^{+*}$ with initial conditions $\mathcal{U}_1(x, t = 0) = 0$ and $\mathcal{U}_2(x, t = 0) = \mathcal{U}_2^{\text{ref}} e^{-\frac{1}{2}\left(\frac{x^2}{(L\delta)^2} - 1\right)}$. Here, L is a characteristic lengthscale and δ is a small parameter, $\delta \ll 1$. Let us consider the point $x = L\delta$, for which we have $\mathcal{U}_2(L\delta, 0) = \mathcal{U}_2^{\text{ref}}$, $\partial_x \mathcal{U}_2(L\delta, 0) = -\frac{\mathcal{U}_2^{\text{ref}}}{L\delta}$, and $\partial_{xx} \mathcal{U}_2(L\delta, 0) \approx \frac{\mathcal{U}_2^{\text{ref}}}{(L\delta)^3}$. Since $\delta \ll 1$, we have

$$\phi_1 \partial_t \mathcal{U}_1(L\delta, 0) \approx \mathsf{A}_{12} \frac{\mathcal{U}_2^{\text{ref}}}{(L\delta)^3}. \tag{4.21}$$

Without loss of generality, we consider $\mathsf{A}_{12} < 0$, so that $\partial_t \mathcal{U}_1(L\delta, 0) < 0$ and, with $\mathcal{U}_1(x, t = 0) = 0$, $\mathcal{U}_1$ becomes negative.

One way to get rid of this issue consists in eliminating the nondiagonal terms in the dispersion matrix and simplifying the problem as is done in (4.16). In Figure 4.2, we plot the results for $\mathcal{U}^{S3eq}$, Pe = 300, and $t = 1$, as a function of σ. We see that, contrary to the model with nondiagonal terms, solutions always remain nonnegative. To further evaluate the effect of removing nondiagonal terms, we plot in Figure 4.3

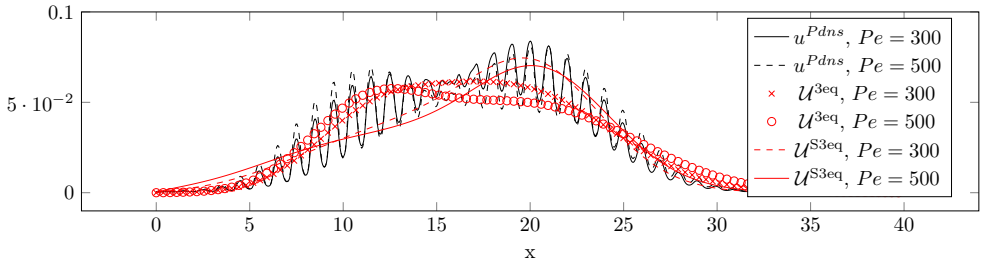

FIG. 4.3. *Comparisons (geometry in Figure* 4.1(e)*) of nondiagonalized* $\mathcal{U}^{3eq}$ *and diagonalized* $\mathcal{U}^{S3eq}$ *models to* u^{Pdns} *for* $Pe = 300$ *and* $Pe = 500$ *at* $t = 10$.

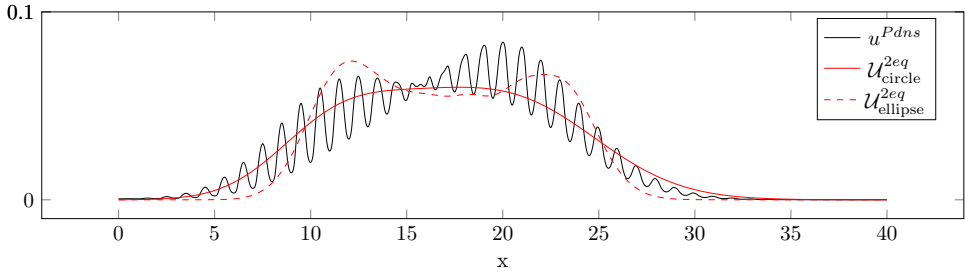

FIG. 4.4. *Comparisons of $\mathcal{U}^{2eq}$ for the circular (Figure* 4.1(b)*) and elliptic (Figure* 4.1(c)*) domain decompositions to u^{Pdns} $Pe = 300$ at $t = 10$.*

$\mathcal{U}^{3eq}$ and $\mathcal{U}^{S3eq}$ (geometry in Figure 4.1(e)), for Pe = 300 and Pe = 500 at $t = 10$, and compare both fields to the reference u^{Pdns}. Comparisons of $\mathcal{U}^{S3eq}$ with u^{Pdns} indicate that the simplified model fails in capturing the bimodal nature of the signal for Pe = 300. However, it is difficult to evaluate further the relative loss in accuracy in diagonalizing from these graphs and we leave that for future work. In the remainder of this work, we focus on the fully coupled nondiagonal models, with the idea that one can use the diagonalized version to maintain positivity but with an accuracy that will need to be assessed.

In Figure 4.4 (geometries in Figure 4.1(b) and (c)), we show that the choice of domain decomposition also has an impact on the fields, with different results for the circular and elliptic central domains. The model based on the ellipse seems to capture the fastest propagating peak of concentration better than the circular decomposition. This difference may stem from the fact that both decompositions sample the distribution of the velocity field differently. For the circular decomposition, one subdomain corresponds to a nonzero velocity, while the other one is the nodule where the velocity is zero. On the other hand, for the elliptic decomposition, part of the low velocity region close to the nodule is included in the subregion. The rationale is that, since the velocities close to the nodule are relatively small, describing the fluid as a unique subdomain may penalize the macroscale model. In this case, we see from Figure 4.4 that the fastest propagating peak of concentration is faster for the elliptic than for the circular decomposition.

More generally, this raises the question of optimal domain decomposition for a given geometry. In more realistic geometries, there can be strong heterogeneities of the velocity or diffusion fields at the microscale. When these fields are distinctly multimodal, the choice of subdomain decomposition is relatively straightforward. However, when this is not the case, specific methods could be developed, for instance, using optimization approaches that minimize a cost function capturing the heterogeneity of the medium or of the velocity field. It is beyond the scope of this paper to study this important issue. In the remainder of this paper, we focus on the impact of the number of phases, which is the focal point of the paper.

4.5.2. Comparison of macroscopic and direct numerical simulation results. We then go on to compare models with one, two (Figure 4.1(b) and (d)), and three (Figure 4.1(e) and (f)) equations for different values of the Pe number in Figure 4.5 ($t = 10$ and $\sigma = 3$). For the one-nodule geometry and small Pe numbers, all models exhibit very similar behaviors and provide an accurate description of the transport at the macroscale. For larger Pe numbers, however, the one-equation description fails to capture the bimodal nature of the scalar field. For the case with

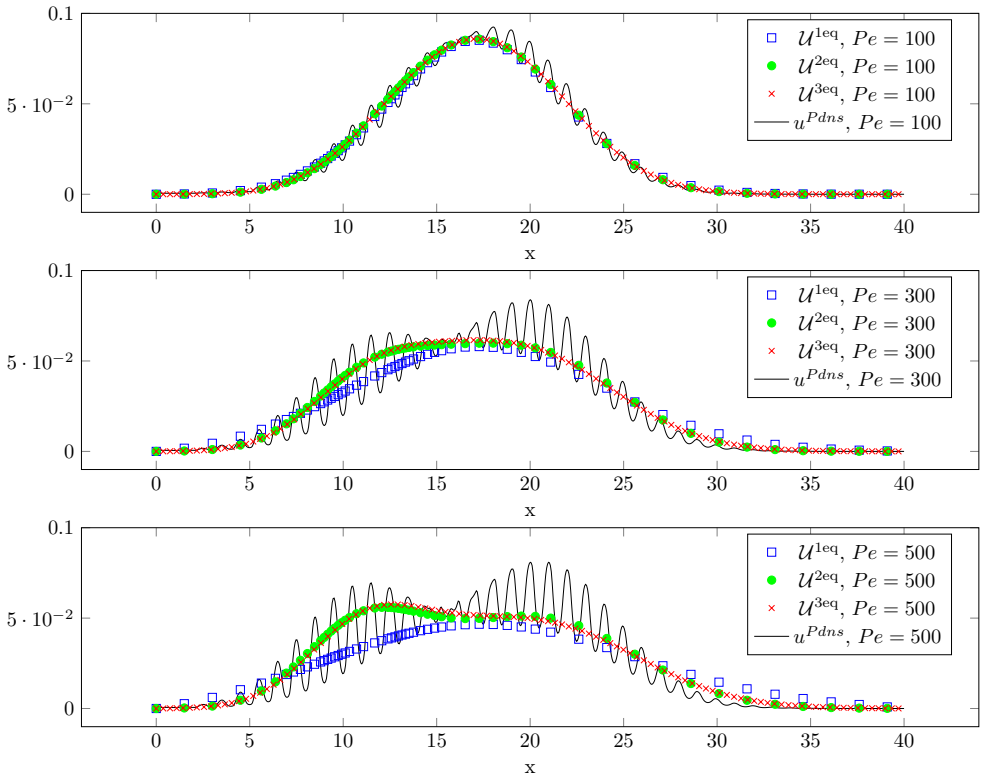

FIG. 4.5. *Comparison of the one-, two- (Figure* 4.1(b)*), and three- (Figure* 4.1(e)*) equation models for the geometry with one nodule,* $t = 10$*,* $\sigma = 3$ *and different Péclet numbers.*

two nodules (Figure 4.6), the one-equation model fails for even lower values of the Péclet number (less than 100) and clearly overestimates the spreading of the signal. This issue, which corresponds to an overestimation of the dispersion coefficient in the short time and preasymptotic regimes, is rather standard with the one-equation model. However, it is important to emphasize that the one-equation model is the usual result from HTs and that it completely fails here. Two- and three-equation descriptions remain very accurate in all cases. The only question is now whether the three-equation model is better than the two-equation one. In the case with one nodule, there is very little difference between the two models. This, we hypothesize, stems from the fact that the geometry displays two, not three, primary subdomains. It is composed of the central nodule, where the scalar is only transported by diffusion, and the fluid, where advection dominates diffusion at large Péclet numbers. We therefore observe an important difference between one- and two-equation formulations, but not between the two- and three-equation models. For the geometry with two nodules, Figure 4.6, we see that the two- and three-equation models display slightly larger differences. This is because the geometry exhibits three distinct regions, with each nodule now being associated with different diffusion coefficients. Even though the differences exist, it is difficult to determine from the average fields whether the two- or the three-equation model is closer to the direct numerical simulations. We will see in the next sections, using reconstructed scalar fields at the microscale, Figures 4.7 and 4.8, that the three-equation model is in fact significantly more accurate.

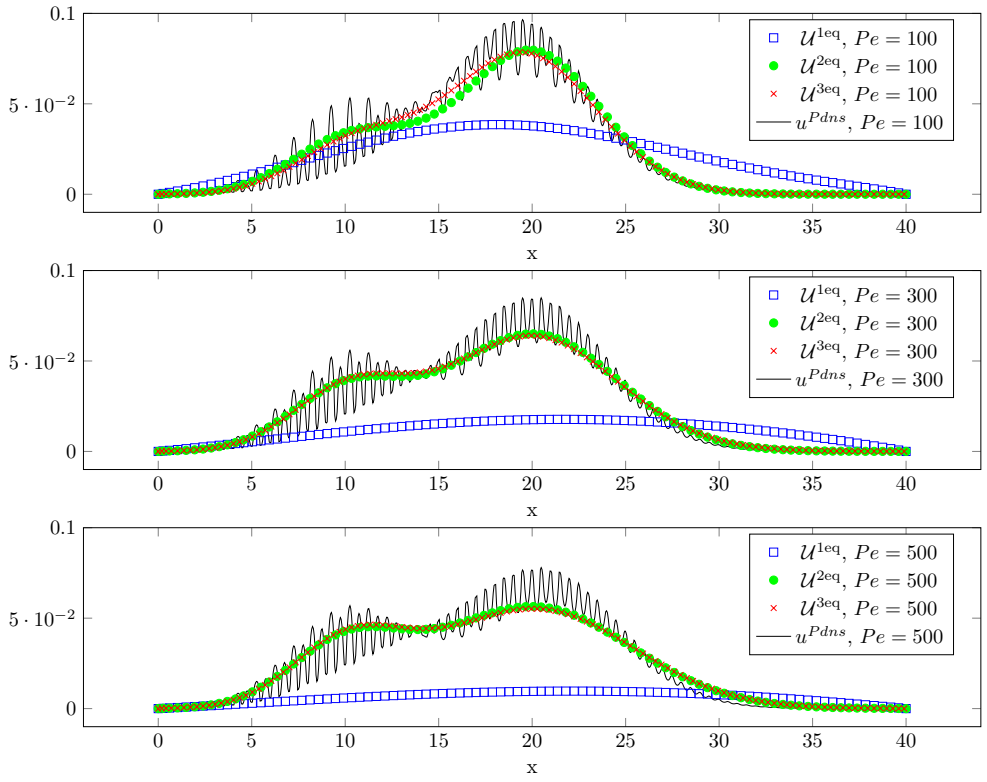

FIG. 4.6. *Comparison of the one-, two- (Figure* 4.1(d)*), and three- (Figure* 4.1(f)*) equation models for the geometry with two nodules,* $t = 10$, $\sigma = 3$ *and different Péclet numbers.*

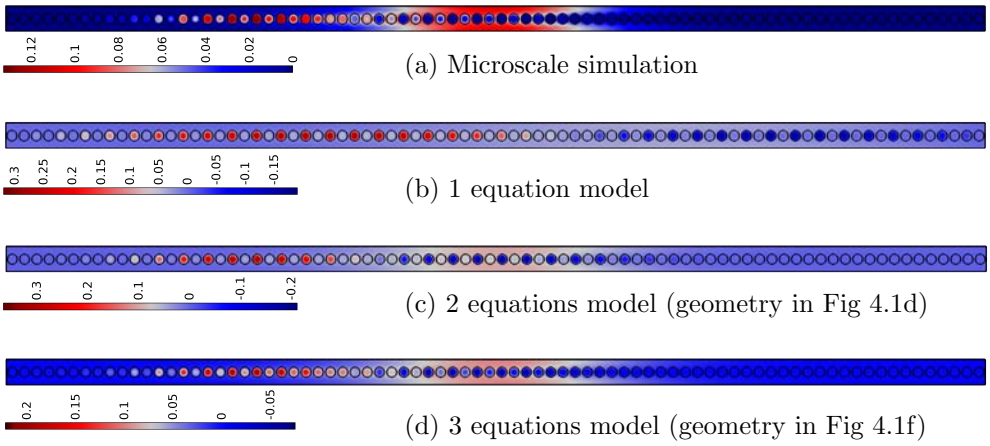

FIG. 4.7. *Reconstructed fields corresponding to the one-, two-, and three-equation models for the geometry with two nodules* $t = 10$, $\sigma = 3$ *and* $Pe = 100$.

4.5.3. Comparison of reconstructed (corrector-type) and direct numerical simulation results. To get a better evaluation of the accuracy of the approximate solution for the perturbations, we now focus on the corrector-type results and microscale reconstructions of the field. We have plotted the reconstructed fields for the case with two nodules for Pe = 100 in Figure 4.7 and Pe = 300 in Figure 4.8

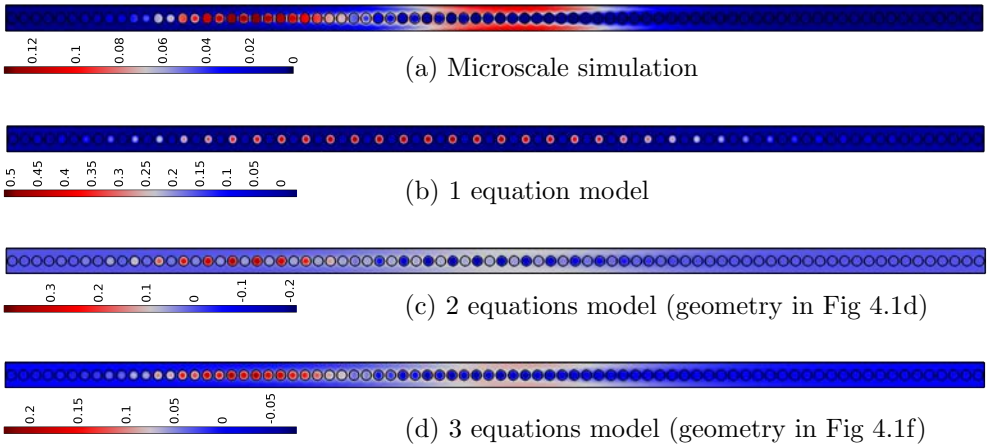

FIG. 4.8. *Reconstructed fields corresponding to the one-, two-, and three-equation models for the geometry with two nodules* $t = 10$, $\sigma = 3$ *and* $Pe = 300$.

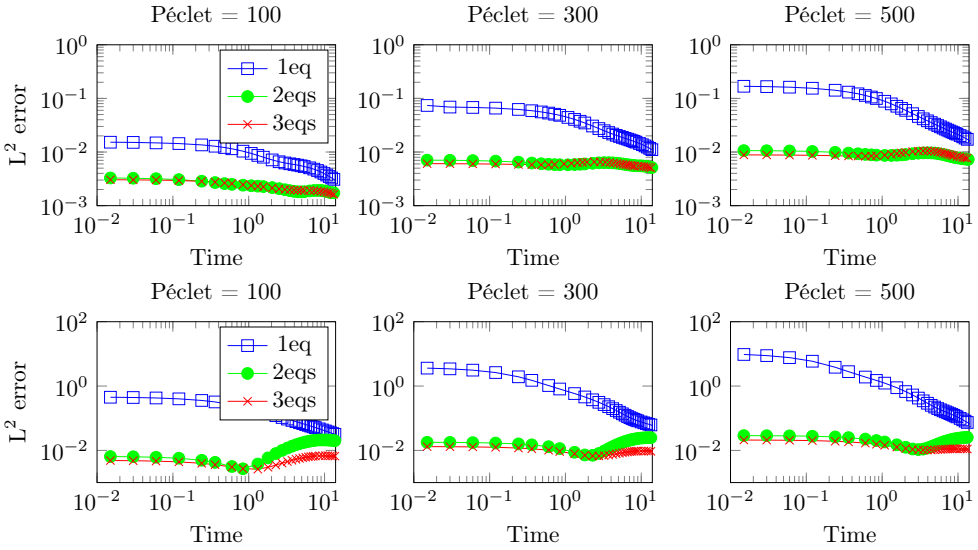

FIG. 4.9. L^2*-norm of the error for Péclet numbers in the set* $\{100, 300, 500\}$ *for the one-, two- (Figure* 4.1(b) *and* (d)*), and three- (Figure* 4.1(e) *and* (f)*) equation models. The first line corresponds to the geometry with one nodule, while the second line describes results for two nodules.*

($t = 10$, $\sigma = 3$). In all cases, the one-equation model completely fails in describing even the most basic features of the fields, whereas the two- and three-equation models are much more accurate. We also see that the approximate form of the perturbation that we have devised can lead to negative values of the scalar field. This is because, although it conserves the zeroth-order moment of the distribution (the integral of u over the whole domain), it does not necessarily respect bounds of the microscale advection-diffusion problem (min/max principles). The three-equation model drastically reduces this issue and provides a better approximation of the extrema than the two-equation model with min/max values that are much closer to the results from the direct numerical simulations.

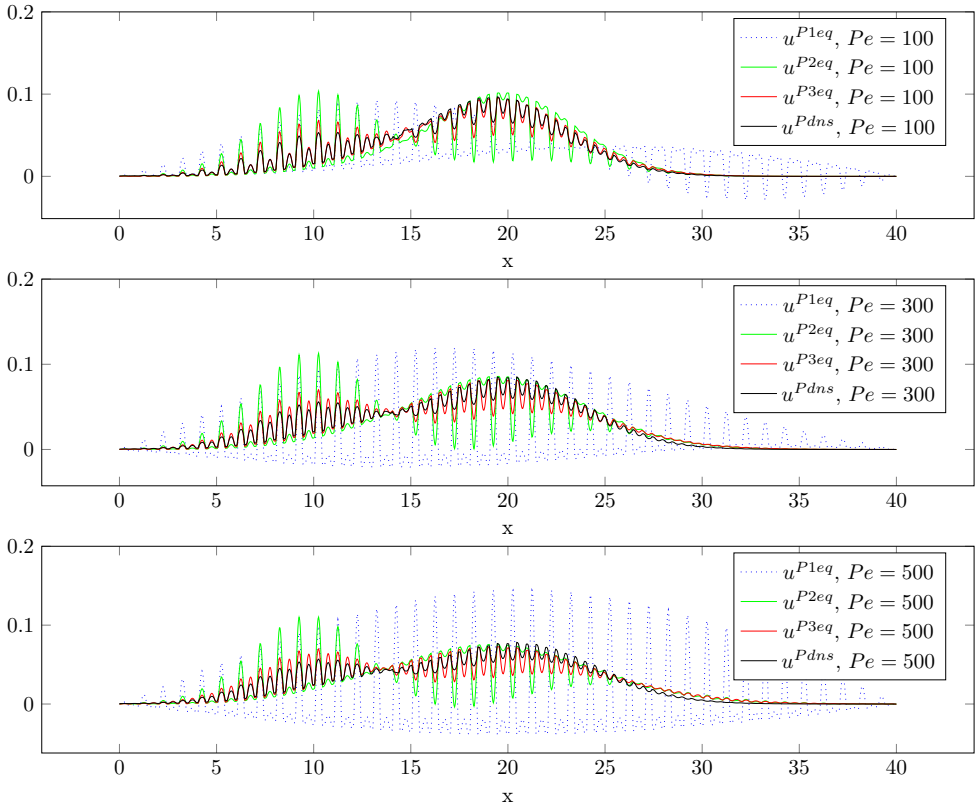

FIG. 4.10. *Projections of the fields for the direct numerical simulations and the reconstructions for the one-, two- (Figure* 4.1(d)*), and three- (Figure* 4.1(f)*) equation models for the geometry with two nodules,* $t = 10$*,* $\sigma = 3$ *and different Péclet numbers.*

We further quantify in Figure 4.9 differences between the models by computing the L^2-norm of the difference between the microscale solution, u^{dns}, and the reconstructed microscale field, u^{Neq},

$$\text{Error} = \sqrt{\int_\Omega \left(u^{dns}(x,y) - u^{Neq}(x,y)\right)^2 dxdy}, \tag{4.22}$$

with an integral over the entire domain Ω. We recover behaviors similar to those we have described earlier, with two- and three-equation descriptions always more accurate than the one-equation model. The three-equation model is always better than the two-equation one, with significant differences only for the case with two nodules. In this figure, we also show that, in the limit of a very short time, the three-equation model is slightly more accurate even for the case with one nodule. Finally, we calculate the projected fields, $u^{PNeq}(x,t) = \int_0^1 u^{Neq}(x,y,t)\,dy$, for all models in Figure 4.10. The main result here is that an approximate solution for perturbations in the three-equation model indeed leads to a more accurate description of the signal.

These results suggest that there may be an optimal number of subdomains, where gain in accuracy balances computational and complexity costs. For instance, in the case with one nodule, we may use two-equation models for practical applications, while three-equation models may be useful for other configurations. Further, this

optimal number of subdomains strongly depends upon the microstructure, the spatial distribution of the parameter fields, the Péclet number, the initial and boundary conditions, or even the time of interest, the size of the macroscopic domain, or the accuracy required. For instance, if we were interested in larger macroscale domains and longer times, even the one-equation model would be accurate. Therefore, the cost function of an optimization problem aiming at determining the optimal number of subdomains would need to be defined specifically for each problem and accuracy required.

5. Conclusions. In this work, we have developed models for the description of scalar transport through heterogeneous media. Standard HTs usually yield one-equation descriptions at the macroscale, which fail in the short time limit and when constraints regarding the dimensionless number are not met (e.g., the Péclet number is too large). Here, we propose an alternative formulation based on a domain decomposition method. The macroscale model consists of a set of coupled equations describing average values of the scalar fields within each subdomain. We have shown that, even for very simple structures, two- or three-equation models overcome important limitations of the standard model. As the number of subdomains increases, so does the accuracy of the description and a decomposition in three subdomains is always better than the one in two subdomains. This work lays the foundation of a theory for finite-epsilon homogenization that shows great potential. However, several aspects must be improved in order to obtain more robust formulations that can be readily used in practical applications. For instance, the approximate form of the solution for the perturbations does not necessarily respect min/max principles for the scalar. Further, the difference between using N and N+1 subdomains may not always be significant and, in many cases, there is probably an optimal number of subdomains, in particular when a clear multimodal distribution of properties can be identified. Another important improvement would be the derivation of a general result for the coercivity of the dispersion matrix, which in our approach must be verified a posteriori for each case. Other improvements include (1) applications to three-dimensional structures with different spatial distributions of properties, (2) decomposition into a larger number of sudomains to assess how the accuracy evolves with a large number of subdomains, (3) optimality of the geometry/topology of the subdomains, and (4) rigorous convergence results with the number of subdomains.

REFERENCES

[1] A. Ahmadi, M. Quintard, and S. Whitaker, *Transport in chemically and mechanically heterogeneous porous media* V*: Two-equation model for solute transport with adsorption*, Adv. Water Resour., 22 (1998), pp. 59–86.

[2] R. Aris, *On the dispersion of a solute in a fluid flowing through a tube*, Proc. A, 235 (1956), pp. 67–77.

[3] J.-L. Auriault, *Taylor dispersion in porous media: Analysis by multiple scale expansions*, Adv. Water Resour., 18 (1995), pp. 217–226.

[4] T. Babey, J.-R. de Dreuzy, and C. Casenave, *Multi-rate mass transfer (MRMT) models for general diffusive porosity structures*, Adv. Water Resour., 76 (2015), pp. 146–156.

[5] A. Bensoussan, J. Lions, and G. Papanicolau, *Asymptotic Analysis for Periodic Structures*, Stud. Math. Appl., Elsevier Science, Amsterdam, 1978.

[6] B. Berkowitz, A. Cortis, M. Dentz, and H. Scher, *Modeling non-Fickian transport in geological formations as a continuous time random walk*, Rev. Geophys., 44 (2006).

[7] B. Berkowitz, H. Scher, and S. E. Silliman, *Anomalous transport in laboratory-scale, heterogeneous porous media*, Water Resour. Res., 36 (2000), pp. 149–158.

[8] B. Bijeljic, A. Raeini, P. Mostaghimi, and M. J. Blunt, *Predictions of non-Fickian solute transport in different classes of porous media using direct simulation on pore-scale images*, Phys. Rev. E, 87 (2013).
[9] H. Brenner, *Dispersion resulting from flow through spatially periodic porous media*, Philos. Trans. R. Soc. A, 297 (1980), pp. 81–133.
[10] H. Brenner and D. A. Edwards, *Macrotransport Processes*, Butterworth-Heineman, Stoneham, UK, 1993.
[11] H. Brezis, *Functional Analysis, Sobolev Spaces and Partial Differential Equations*, Springer-Verlag, New York, 2011.
[12] P. Chatwin, *The approach to normality of the concentration distribution of a solute in a solvent flowing along a straight pipe*, J. Fluid Mech., 43 (1970), pp. 321–352.
[13] F. Cherblanc, A. Ahmadi, and M. Quintard, *Two-medium description of dispersion in heterogeneous porous media: Calculation of macroscopic properties*, Water Resour. Res., 39 (2003), pp. 1154–1173.
[14] F. Cherblanc, A. Ahmadi, and M. Quintard, *Two-domain description of solute transport in heterogeneous porous media: Comparison between theoretical predictions and numerical experiments*, Adv. Water Resour., 30 (2007), pp. 1127–1143.
[15] K. H. Coats and B. D. Smith, *Dead-end pore volume and dispersion in porous media*, Soc. Petroleum Engineers J., March (1964), pp. 73–84.
[16] J. H. Cushman, L. S. Bennethum, and B. X. Hu, *A primer on upscaling tools for porous media*, Adv. Water Resour., 25 (2002), pp. 1043–1067.
[17] J. H. Cushman and T. R. Ginn, *Nonlocal dispersion in media with continuously evolving scales of heterogeneity*, Transp. Porous Media, 13 (1993), pp. 123–138.
[18] Y. Davit, C. G. Bell, H. M. Byrne, L. A. C. Chapman, L. S. Kimpton, G. E. Lang, K. H. L. Leonard, J. M. Oliver, N. C. Pearson, R. J. Shipley, S. L. Waters, J. P. Whiteley, B. D. Wood, and M. Quintard, *Homogenization via formal multiscale asymptotics and volume averaging: How do the two techniques compare?*, Adv. Water Resour., 62 (2013), pp. 178–206.
[19] Y. Davit and M. Quintard, *Comment on Frequency-dependent dispersion in porous media*, Phys. Rev. E, 86 (2012), pp. 1–4.
[20] Y. Davit and M. Quintard, *Theoretical Analysis of Transport in Porous Media: Multi-equation and Hybrid Models for a Generic Transport Problem with Nonlinear Source Terms*, in Handbook of Porous Media, 3rd ed., K. Vafai, ed., CRC Press, Boca Raton, FL, 2015.
[21] Y. Davit and M. Quintard, *Technical notes on volume averaging in porous media* I*: How to choose a spatial averaging operator for periodic and quasiperiodic structures*, Transp. Porous Media, 119 (2017), pp. 555–584.
[22] J.-R. de Dreuzy, A. Rapaport, T. Babey, and J. Harmand, *Influence of porosity structures on mixing-induced reactivity at chemical equilibrium in mobile/immobile multi-rate mass transfer (MRMT) and multiple interacting continua (MINC) models*, Water Resour. Res., 49 (2013), pp. 8511–8530.
[23] M. Dentz, A. Cortis, H. Scher, and B. Berkowitz, *Time behavior of solute transport in heterogeneous media: Transition from anomalous to normal transport*, Adv. Water Resour., 27 (2004), pp. 155–173.
[24] V. Giovangigli, *Multicomponent Flow Modeling*, Birkhäuser, Boston, 1999.
[25] P. Gouze, Y. Melean, T. Le Borgne, M. Dentz, and J. Carrera, *Non-Fickian dispersion in porous media explained by heterogeneous microscale matrix diffusion: Non-Fickian dispersion and heterogeneous diffusion*, Water Resour. Res., 44 (2008).
[26] W. G. Gray, A. Leijnse, R. L. Kolar, and C. A. Blain, *Mathematical Tools for Changing Spatial Scales in the Analysis of Physical Systems*, CRC Press, Boca Raton, FL, 1993.
[27] R. Haggerty and S. M. Gorelick, *Multiple-rate mass transfer for modelling diffusion and surface reactions in media with pore-scale heterogeneity*, Water Resour. Res., 31 (1995), pp. 2383–2400.
[28] N. J. Higham, *Computing a nearest symmetric positive semidefinite matrix*, Linear Algebra Appl., 103 (1988), pp. 103–118.
[29] U. Hornung, *Miscible displacement in porous media influenced by mobile and immobile water*, Rocky Mountain J. Math., 21 (1991), pp. 645–669.
[30] U. Hornung, ed., *Homogenization and Porous Media*, Springer-Verlag, New York, 1997.
[31] D. L. Koch and J. F. Brady, *A non-local description of advection-diffusion with application to dispersion in porous media*, J. Fluid Mech., 180 (1987), pp. 387–403.
[32] P. Landereau, B. Noetinger, and M. Quintard, *Quasi-steady two-equation models for diffusive transport in fractured porous media: Large-scale properties for densely fractured systems*, Adv. Water Resour., 24 (2001), pp. 863–876.

[33] M. Levy and B. Berkowitz, *Measurement and analysis of non-Fickian dispersion in heterogeneous porous media*, J. Contaminant Hydrology, 64 (2003), pp. 203–226.
[34] C. M. Marle, *On macroscopic equations governing multiphase flow with diffusion and chemical reactions in porous media*, Internat. J. Engrg. Sci., 20 (1982), pp. 643–662.
[35] C. Moyne, *Two-equation model for a diffusive process in porous media using the volume averaging method with an unsteady state closure*, Adv. Water Resour., 20 (1997), pp. 63–76.
[36] S. P. Neuman and D. M. Tartakovsky, *Perspective on theories of non-Fickian transport in heterogeneous media*, Adv. Water Resour., 32 (2009), pp. 670–680.
[37] M. Prat, *Some refinements concerning the boundary conditions at the macroscopic level*, Transp. Porous Media, 7 (1992), pp. 147–161.
[38] M. Quintard and S. Whitaker, *One- and two-equation models for transient diffusion processes in two-phase systems*, in Advances in Heat Transfer, Academic Press, New York, 1993, pp. 369–464.
[39] M. Quintard and S. Whitaker, *Transport in ordered and disordered porous media* I*: The cellular average and the use of weighting functions*, Transp. Porous Media, 14 (1994), pp. 163–177.
[40] M. Quintard and S. Whitaker, *Transport in ordered and disordered porous media* II*: Generalized volume averaging*, Transp. Porous Media, 14 (1994), pp. 179–206.
[41] M. Quintard and S. Whitaker, *Transport in ordered and disordered porous media* III*: Closure and comparison between theory and experiment*, Transp. Porous Media, 15 (1994), pp. 31–49.
[42] M. Quintard and S. Whitaker, *Transport in ordered and disordered porous media* IV*: Computer generated porous media for three-dimensional systems*, Transp. Porous Media, 15 (1994), pp. 51–70.
[43] M. Quintard and S. Whitaker, *Transport in ordered and disordered porous media* V*: Geometrical results for two-dimensional systems*, Transp. Porous Media, 15 (1994), pp. 183–196.
[44] M. Quintard and S. Whitaker, *Theoretical analysis of transport in porous media*, in Handbook of Heat Transfer in Porous Media, Marcel Decker, New York, 2000, pp. 1–52.
[45] J. Salles, J.-F. Thovert, R. Delannay, L. Prevors, J.-L. Auriault, and P. Adler, *Taylor dispersion in porous media, determination of the dispersion tensor*, Phys. Fluids A, 15 (1993), pp. 2348–2376.
[46] E. Sanchez-Palencia, *Non-homogeneous Media and Vibration Theory*, Lecture Notes in Phys. 127, Springer-Verlag, New York, 1980.
[47] C. Soulaine, Y. Davit, and M. Quintard, *A two-pressure model for slightly compressible single phase flow in bi-structured porous media*, Chemical Engineering Science, 96 (2013), pp. 55–70.
[48] L. Tartar, *The General Theory of Homogenization: A Personalized Introduction*, Springer-Verlag, New York, 2009.
[49] R. Taylor and R. Krishna, *Multicomponent Mass Transfer*, John Wiley & Sons, New York, 1993.
[50] S. G. Taylor, *Dispersion of soluble matter in solvent flowing slowly through a tube*, Proc. Roy. Soc. London, 219 (1953), pp. 186–203.
[51] V. K. Vanag and I. R. Epstein, *Cross-diffusion and pattern formation in reaction-diffusion systems*, Phys. Chem. Chem. Phys., 11 (2009), pp. 897–912.
[52] S. Whitaker, *The Method of Volume Averaging*, Theory Appl. Transp. Porous Media 13, Springer Netherlands, Dordrecht, 1999.
[53] M. Willmann, J. Carrera, X. Sanchez-Vila, O. Silva, and M. Dentz, *Coupling of mass transfer and reactive transport for nonlinear reactions in heterogeneous media: Coupling of mass transfer and reactive transport*, Water Resour. Res., 46 (2010).
[54] Z. Wu and G. Q. Chen, *Approach to transverse uniformity of concentration distribution of a solute in a solvent flowing along a straight pipe*, J. Fluid Mech., 740 (2014), pp. 196–213.
[55] Z. Wu, X. Fu, and G. Wang, *On spatial pattern of concentration distribution for Taylor dispersion process*, Sci. Rep., 6 (2016).